


Quantum geometry and geometric entanglement entropy of one-dimensional Floquet topological matter

Longwen Zhou ^{*}

College of Physics and Optoelectronic Engineering, Ocean University of China, Qingdao, China 266100;
Key Laboratory of Optics and Optoelectronics, Qingdao, China 266100;
and Engineering Research Center of Advanced Marine Physical Instruments and Equipment of MOE, Qingdao, China 266100



(Received 20 May 2024; revised 7 July 2024; accepted 6 August 2024; published 14 August 2024)

The geometry of quantum states could offer indispensable insights for characterizing the topological properties, phase transitions, and entanglement nature of many-body systems. In this work, we reveal the quantum geometry and the associated entanglement entropy (EE) of Floquet topological states in one-dimensional periodically driven systems. The quantum metric tensors of Floquet states are found to show nonanalytic signatures at topological phase transition points. Away from the transition points, the bipartite geometric EE of Floquet states exhibits an area-law scaling vs the system size, which holds for a Floquet band at any filling fractions. For a uniformly filled Floquet band, the EE further becomes purely quantum geometric. At phase transition points, the geometric EE scales logarithmically with the system size and displays cusps in the nearby parameter ranges. These discoveries are demonstrated by investigating typical Floquet models including periodically driven spin chains, Floquet topological insulators, and superconductors. Our findings uncover the rich quantum geometries of Floquet states, unveiling the geometric origin of EE for gapped Floquet topological phases, and introducing information-theoretic means of depicting topological transitions in Floquet systems.

DOI: [10.1103/PhysRevB.110.054310](https://doi.org/10.1103/PhysRevB.110.054310)

I. INTRODUCTION

Floquet topological phases have attracted sustained research interest over the last decades [1–9]. It was found that periodic driving fields could endue a system with rich and unique features that are absent or challenging to achieve in static systems, such as Floquet phases with large topological invariants and many topological edge states [10], dispersionless Floquet edge modes at quasienergy π [11], or anomalous chiral edge modes encircling the quasienergy Brillouin zone (BZ) [12], and exotic phenomena like Floquet-band holonomy [13] and integer quantum Hall effect from chaos [14]. Experimental realizations of these intriguing physics in both solid-state materials and quantum simulators [15–30] brought about their potential applications in topological photonic devices [31–33], ultrafast electronics [4,8], and novel quantum computing strategies [34,35].

In contrast with topological aspects, less attention was paid to the geometric properties of Floquet states [36] and their resulting entanglement characteristics [37]. The geometries of quantum states, including the amplitude and phase distances described, respectively, by the quantum metric and Berry curvature tensors [38], have played pivotal roles in the study of Bloch-electron dynamics [39], topological states of matter [40], and quantum phase transitions [41–43]. For example, the integration of Berry curvature over a two-dimensional BZ yields the first Chern number of a Bloch band, which serves as the topological origin of various transport phenomena including the integer quantum Hall effect [44], quantum

anomalous Hall effect [45], and quantized adiabatic charge pumping [46]. The quantum metric tensor could instead appear in the high-order response coefficient of electrons to external fields [47] and the superfluid weight of flat bands [48], yielding important insights for the understanding of nonlinear Hall effects [49] and flat-band superconductivity in correlated materials [50]. In periodically driven systems, the quantum geometry of Floquet bands may also offer essential information about the topological and entanglement features of the underlying nonequilibrium states. First, as Floquet bands could weave around the first quasienergy BZ $E \in [-\pi, \pi)$, they may develop level crossings at both the quasienergies zero and π , yielding two possible flavors of topological phase transitions [11]. Whether and how these transitions would leave unique signals in the quantum geometric tensor of Floquet states then constitute interesting issues to address. Second, driving fields could generate long-range couplings in a system and allow Floquet bands to carry large topological invariants [10]. Unveiling geometric aspects of these quasienergy bands with large topological numbers may help us to deepen our understanding of the quantum transport in driven systems. Third, Floquet systems could possess anomalous topological phases with unique edge states, such as degenerate edge modes at the quasienergy π [12], which are not reachable in static settings. Geometric signatures of these anomalous Floquet topological phases deserve to be further clarified. Resolving these issues thus forms an indispensable part for our understanding of Floquet topological matter and their entanglement properties.

In this paper, we uncover the quantum geometries of Floquet-Bloch bands and their associated entanglement nature in one-dimensional (1D) Floquet topological phases. In

^{*}zhoulw13@u.nus.edu

Sec. II, we outline the generic definitions of Abelian quantum geometric tensor and geometric entanglement entropy (GEE) of Floquet states, with further theoretical details presented in Appendixes A–E. Based on these definitions, we obtain the quantum metric tensor (QMT) and GEE of typical 1D Floquet systems including periodically driven spin chains, Floquet topological insulators, and superconductors in Secs. III–V. Throughout these model studies, we reveal that the integrated QMT of a filled Floquet band would show nonanalytic signatures when the system undergoes a transition between different Floquet topological phases. Moreover, away from the transition point, the GEE always follow an area-law scaling vs the system size irrespective of the filling fraction of the considered Floquet band, and the bipartite EE becomes purely geometric when the Floquet band is uniformly filled. At the transition point between different Floquet topological phases, the EE is also of geometric origin and further follows a log-law scaling vs the system size, as expected in 1D critical metallic phases. In Sec. VI, we summarize our results and discuss potential directions of future research.

II. QUANTUM GEOMETRY AND GEOMETRIC ENTANGLEMENT ENTROPY

In this section, we outline the definitions of key quantum geometric objects and their related entanglement measures that will be investigated in this study. Further derivation details of these quantities are given in the Appendixes A–E.

Consider a set of normalized quantum states $\{|\psi(\mathbf{k})\rangle\}$, which are defined in a continuous D -dimensional parameter space $\mathbf{k} = (k_1, k_2, \dots, k_D)$. The infinitesimal distance between any two nearby states in such a \mathbf{k} space can be expressed as $ds^2 \equiv 1 - |\langle\psi(\mathbf{k})|\psi(\mathbf{k} + d\mathbf{k})\rangle|^2$, which is equal to one (zero) if the states $|\psi(\mathbf{k})\rangle$ and $|\psi(\mathbf{k} + d\mathbf{k})\rangle$ are orthogonal (identical up to a phase factor). Retaining terms up to the second order in $d\mathbf{k}$, we can equivalently write ds^2 as

$$ds^2 = \text{Re}[\mathcal{Q}_{\alpha\beta}(\mathbf{k})]dk_\alpha dk_\beta = g_{\alpha\beta}(\mathbf{k})dk_\alpha dk_\beta, \quad (1)$$

where the indices $\alpha, \beta = 1, 2, \dots, D$ are summed over. The quantity $\mathcal{Q}_{\alpha\beta}(\mathbf{k})$, given by

$$\mathcal{Q}_{\alpha\beta}(\mathbf{k}) = \langle\partial_{k_\alpha}\psi(\mathbf{k})|[1 - |\psi(\mathbf{k})\rangle\langle\psi(\mathbf{k})|]|\partial_{k_\beta}\psi(\mathbf{k})\rangle, \quad (2)$$

is usually referred to as the component of quantum geometric tensor (QGT). The real part of QGT gives the QMT [51], whose components are given by the $g_{\alpha\beta}(\mathbf{k})$ in Eq. (1). The integration of QMT over \mathbf{k} space may provide further diagnoses for level crossings and quantum phase transitions in the system [52]. The imaginary part of QGT yields the Berry curvature $\mathcal{F}(\mathbf{k})$ [53], whose components are

$$\mathcal{F}_{\alpha\beta}(\mathbf{k}) = -2 \text{Im}[\mathcal{Q}_{\alpha\beta}(\mathbf{k})]. \quad (3)$$

The Berry curvature of Bloch bands determines the anomalous dynamics and quantized Hall response of electrons in two-dimensional systems [39]. The integration of $\mathcal{F}_{\alpha\beta}(\mathbf{k})$ over a closed and orientable two-dimensional \mathbf{k} -space manifold further yields the first Chern number, which is a key ingredient in characterizing topological phases of matter [40]. The information provided by $g_{\alpha\beta}(\mathbf{k})$ and $\mathcal{F}_{\alpha\beta}(\mathbf{k})$ thus offers a complete description for the geometry of quantum states $\{|\psi(\mathbf{k})\rangle\}$ in \mathbf{k} space. Note in passing that for a 1D \mathbf{k} space, the Berry

curvature vanishes by definition and the QGT reduces to a one-component QMT, i.e.,

$$g_{kk} = \langle\partial_k\psi(k)|[1 - |\psi(k)\rangle\langle\psi(k)|]|\partial_k\psi(k)\rangle. \quad (4)$$

In Appendix B, the expressions of g_{kk} for generic 1D two-band models and for some representative examples are worked out explicitly, with k being identified as the 1D quasi-momentum defined in the first BZ $[-\pi, \pi)$. These expressions will be used to characterize the quantum geometry of Floquet-Bloch bands in later sections.

Quantum entanglement comprises the nonclassical correlations among different constituents of a composite quantum system. Related information-theoretic measures, such as the entanglement spectrum and EE, have been regularly adopted in depicting quantum phase transitions and topological phases in many-body systems (for reviews see [54–64]). In a recent study, it was found that the geometry of quantum states could contribute a universal area-law component to the bipartite EE of noninteracting fermions in static multiband models [65]. Such a geometric entanglement entropy may be defined as

$$S_{\text{QG}} \equiv S_A - S_{A_0}, \quad (5)$$

where S_A is the (Rényi or von Neumann) EE between the subsystem A and its complementary \bar{A} in a bipartite system $A \cup \bar{A}$ with fermions populating a Bloch band. S_{A_0} encompasses the bipartite EE of fermions sharing the same Fermi surface with those in the system $A \cup \bar{A}$ but with trivial Bloch band geometries. The difference between S_A and S_{A_0} then yields an entropic component originated from the inherent quantum geometry of occupied Bloch states [65].

For electrons in a 1D periodic lattice with L unit cells, the S_{A_0} can be obtained rather generally from the spectrum of overlap matrix O^{A_0} among plane-wave basis $\{|n\rangle|k\rangle = L^{-1/2}e^{ikn}|n = 1, \dots, L\rangle$, whose matrix elements are given by

$$O_{k,k'}^{A_0} = \frac{1}{L} \sum_{n \in A} e^{-i(k-k')n}. \quad (6)$$

Here L is the total number of unit cells in the composite system $A \cup \bar{A}$, and the cell index n has been restricted to the subsystem A . k and k' are wave vectors running over all the occupied single-particle eigenbases, so that O^{A_0} is an $N \times N$ matrix if there are N particles in the system $A \cup \bar{A}$. Denoting the eigenvalues of O^{A_0} by $\{\eta_{\ell 0} | \ell = 1, \dots, N\}$, we can obtain the von Neumann EE S_{A_0} in Eq. (5) as [66–68]

$$S_{A_0} = - \sum_{\ell=1}^N [\eta_{\ell 0} \ln \eta_{\ell 0} + (1 - \eta_{\ell 0}) \ln(1 - \eta_{\ell 0})], \quad (7)$$

with further derivation details presented in Appendixes C–E. Meanwhile, if $\{|\psi_k\rangle\}$ constitutes the occupied eigenstates of a Bloch band in the system $A \cup \bar{A}$, we can construct an overlap matrix O^A among the states in $\{|\psi_k\rangle\}$. Its matrix elements (after being restricted to the subsystem A) are given by

$$O_{k,k'}^A = \frac{1}{L} \sum_{n \in A} e^{-i(k-k')n} \langle\psi_k|\psi_{k'}\rangle. \quad (8)$$

With N particles in the system, O^A is also $N \times N$ with N eigenvalues $\{\eta_\ell | \ell = 1, \dots, N\}$, from which the von Neumann

bipartite EE in Eq. (5) can be obtained as [66–68]

$$S_A = - \sum_{\ell=1}^N [\eta_\ell \ln \eta_\ell + (1 - \eta_\ell) \ln(1 - \eta_\ell)]. \quad (9)$$

Further derivation details of S_A can also be found in Appendixes C–E. Note in passing that, formally speaking, both the S_{A_0} and S_A in Eqs. (7) and (9) do not explicitly depend on the size of subsystem A . Within a Bloch band, all the nontrivial quantum geometries of the occupied states $\{|\psi_k\rangle\}$ are encoded in their overlaps $\langle\psi_k|\psi_{k'}\rangle$ with $k \neq k'$. We thus expect that the difference between S_A and S_{A_0} in Eq. (5) could properly describe a quantum geometric component of EE, as the trivial contribution S_{A_0} (from a free-fermion gas in a periodic lattice without onsite potentials) has been removed (see Appendixes C–E from further discussions). It was also revealed that for fermions filling a gapped Bloch band, both S_A and S_{A_0} scale as $L_A^{D-1} \ln L_A$ vs the subsystem size L_A up to its leading order, with the same scaling coefficient in D spatial dimensions [69]. Their difference should thus follow an area-law scaling vs L_A when the system is away from its critical point. One may then identify quantum and topological phase transitions from the change of finite-size scaling behaviors in S_{QG} .

A Floquet quantum system can be described by a Hamiltonian $\hat{H}(t) = \hat{H}(t + T)$, which is periodic in time t with the driving period T . If we are interested in the stroboscopic dynamics of the system, we can focus on its Floquet operator $\hat{U} = \hat{T} e^{-i \int_0^T \hat{H}(t') dt'}$, which controls the evolution of the system over a complete driving period (\hat{T} performs the

time ordering). The eigenvectors and eigenphases of \hat{U} are, respectively, called the Floquet eigenstates and quasienergies, which could be obtained by solving the eigenvalue equation $\hat{U}|\psi\rangle = e^{-iE}|\psi\rangle$. The Floquet eigenstates form a complete and orthonormal basis of the system. If $\hat{H}(t)$ also possesses some discrete spatial translational symmetries, \hat{U} will hold the same symmetries. Its quasienergies could then be grouped into bands confined in the first quasienergy BZ $E \in [-\pi, \pi)$, which are called the Floquet-Bloch bands. In this case, a Floquet eigenstate $|\psi_j(\mathbf{k})\rangle$ in the quasienergy band $E_j(\mathbf{k})$ satisfies the equation $\hat{U}|\psi_j(\mathbf{k})\rangle = e^{-iE_j(\mathbf{k})}|\psi_j(\mathbf{k})\rangle$, with j the band index and \mathbf{k} the quasimomentum. In Appendixes C–E, we demonstrate that for fermions filling the Floquet-Bloch band of a 1D periodically driven system, the formalism of QMT and GEE as outlined in this section are also applicable after the replacement of each filled Bloch state with a Floquet-Bloch eigenstate at a given quasienergy in the related equations. This allows us to unveil the quantum geometry and the associated EE of some representative 1D periodically driven systems, including Floquet spin chains, topological insulators, and superconductors in the following sections.

III. HARMONICALLY DRIVEN SPIN CHAIN: QMT AND GEE

We start with a “minimal” Floquet model, whose geometric, topological, and entanglement properties could be controlled by periodic driving fields. The model describes a 1D spin chain subject to harmonic drivings [70], whose Hamiltonian takes the form

$$\hat{H}(t) = \sum_n \left\{ \frac{\delta_1 [1 - \sin(\omega t)]}{4} \hat{\sigma}_n^x \hat{\sigma}_{n+1}^x + \frac{\delta_1 [1 + \sin(\omega t)]}{4} \hat{\sigma}_n^y \hat{\sigma}_{n+1}^y \right\} - \sum_n \frac{\delta_1 \cos(\omega t)}{4} (\hat{\sigma}_n^x \hat{\sigma}_{n+1}^y + \hat{\sigma}_n^y \hat{\sigma}_{n+1}^x) - \frac{\delta_2}{2} \sum_n \hat{\sigma}_n^z. \quad (10)$$

Here δ_1 controls the driving amplitude and ω is the driving frequency. δ_2 describes the amplitude of magnetic field along z axis. $\hat{\sigma}_n^{x,y,z}$ are Pauli matrices of quantum spin- $\frac{1}{2}$ variables on the n th lattice site. In a former work [70], this model has been experimentally realized to study Floquet dynamical quantum phase transitions and establish their relations with Floquet topological phases. Performing Jordan-Wigner and Fourier transformations sequentially under the periodic boundary condition (PBC), we can express $\hat{H}(t)$ in the Nambu spinor representation as $\hat{H}(t) = \sum_k \hat{\Psi}_k^\dagger H(k, t) \hat{\Psi}_k$, where $k \in [-\pi, \pi)$ is the quasimomentum and [70]

$$H(k, t) = d_x(k) [\cos(\omega t) \sigma_x + \sin(\omega t) \sigma_y] + d_z(k) \sigma_z. \quad (11)$$

Here $\sigma_{x,y,z}$ are Pauli matrices in their usual representations and

$$d_x(k) = \frac{\delta_1 \sin k}{2}, \quad d_z(k) = \frac{\delta_1 \cos k + \delta_2}{2}. \quad (12)$$

Applying a rotation $|\psi(k, t)\rangle = U_R(t)|\varphi(k, t)\rangle$ to the evolving state in the Schrödinger equation $i\partial_t |\psi(k, t)\rangle = H(k, t)|\psi(k, t)\rangle$, we could describe the dynamics of rotated state $|\varphi(k, t)\rangle$ by the equation $i\partial_t |\varphi(k, t)\rangle = H(k)|\varphi(k, t)\rangle$ with a time-independent Floquet-Bloch effective Hamiltonian

$H(k)$, where $U_R(t) = \text{diag}(1, e^{i\omega t})$ and

$$H(k) = h_0 \sigma_0 + h_x(k) \sigma_x + h_z(k) \sigma_z, \quad (13)$$

with $h_0 = \omega/2$,

$$h_x(k) = d_x(k), \quad h_z(k) = d_z(k) - \frac{\omega}{2}, \quad (14)$$

and σ_0 denotes the 2×2 identity matrix. Due to the time periodicity of $U_R(t) = U_R(t + T)$ with $T = 2\pi/\omega$, the stroboscopic dynamics of the system is fully governed by $H(k)$, whose quasienergy bands have the dispersions described by Eq. (A2) with

$$E(k) = \sqrt{h_x^2(k) + h_z^2(k)} \quad \text{mod } 2\pi. \quad (15)$$

Note in passing that the term $h_0 \sigma_0$ in Eq. (13) is generated by the rotating-frame transformation $U_R(t)$. As $h_0 \sigma_0$ is proportional to the identity and independent of k , it does not affect the geometric and topological properties of Floquet states in our system. In the meantime, if we go back to the original time frame and consider a one-period evolution starting at $t = 0$, the Floquet operator of the system becomes $U(k) = e^{-ih_0 T \sigma_0} e^{-i(h_x \sigma_x + h_z \sigma_z) T} = -e^{-i(h_x \sigma_x + h_z \sigma_z) T}$, which possesses the

chiral symmetry σ_y as $\sigma_y U(k) \sigma_y = U^\dagger(k)$ [70]. We also notice that in the quasienergy dispersion $E(k)$, $h_z(k)$ depends on the driving frequency ω due to Eq. (14), making $E(k)$ obviously different from the energy spectrum of the static model. We can now obtain the QMT and GEE of the system following Appendixes A–E. Plugging Eqs. (12), (14), and (15) into (B7), we find the QMT as

$$g_{kk} = g_{kk}^\pm = \frac{(1 + \mu \cos k)^2}{4(1 + \mu^2 + 2\mu \cos k)^2}. \quad (16)$$

Here we have set the driving amplitude δ_1 as the unit of energy and introduced the shorthand notation $\mu = (\delta_2 - \omega)/\delta_1$. Since $g_{kk} \geq 0$, we can find its integrated contribution G over the whole BZ, i.e.,

$$G = \int_{-\pi}^{\pi} \frac{dk}{2\pi} g_{kk} = \begin{cases} \frac{1}{8(\mu^2-1)}, & |\mu| > 1 \\ \frac{\mu^2-2}{8(\mu^2-1)}, & |\mu| < 1. \end{cases} \quad (17)$$

It is clear that the integrated QMT is divergent at $|\mu| = 1$, i.e., at $|\delta_2 - \omega| = |\delta_1|$, where we have $E = 0$ in Eq. (15) and the two Floquet bands $\omega/2 \pm E$ meet with each other at the quasienergy $\omega/2$, which is the edge of the first quasienergy BZ. Quantum phase transitions unique to Floquet systems could then happen at $\mu = \pm 1$, which are further associated with transitions between different Floquet topological phases [70]. The locations of these transition points are controlled by the driving frequency ω . The divergence of G at $\mu = \pm 1$ then offers clear geometric signatures for the Floquet topological phase transitions in our system.

Away from the transition points, we find the limiting behaviors of G as

$$\lim_{\mu \rightarrow 0} G = \frac{1}{4}, \quad \lim_{\mu \rightarrow \infty} G = 0. \quad (18)$$

In Ref. [70], it was found that the system belongs to a topologically nontrivial (trivial) phase when $|\mu| < 1$ ($|\mu| > 1$). Therefore, the integration of GMT shows different limiting behaviors in the topological and trivial limits of the system, offering another geometric probe to distinguish these different Floquet phases. Approaching the transition point, we find

$$\lim_{\mu \rightarrow \pm 1} G \rightarrow \frac{1}{16} |\mu \mp 1|^{-\nu}, \quad (19)$$

with the critical exponent $\nu = 1$. In Fig. 1, we present the integrated QMT for a typical set of system parameters, which clearly demonstrates its critical properties around phase transition points ($\mu = \pm 1$) and limiting behaviors in different Floquet topological phases.

Next, to obtain the GEE, we combine Eqs. (12), (14), and (15) into (A7), yielding the overlap of wave functions in the Floquet band with dispersion $\omega/2 - E(k)$, i.e.,

$$\langle \psi_k | \psi_{k'} \rangle = \frac{h_x(k)h_x(k') + [E(k) - h_z(k)][E(k') - h_z(k')]}{2\sqrt{E(k)E(k')}[E(k) - h_z(k)][E(k') - h_z(k)]}}, \quad (20)$$

where $k, k' = 2\pi\ell/L$ and $\ell = 1, \dots, N$, with L being the number of unit cells and $N \leq L$ being the number of occupied single-particle orbitals in the multiparticle Floquet state $|\Psi\rangle = \prod_k |\psi_k\rangle$ of our system. For example, when $N = L$, the lower Floquet band with quasienergy dispersion $\omega/2 - E(k)$

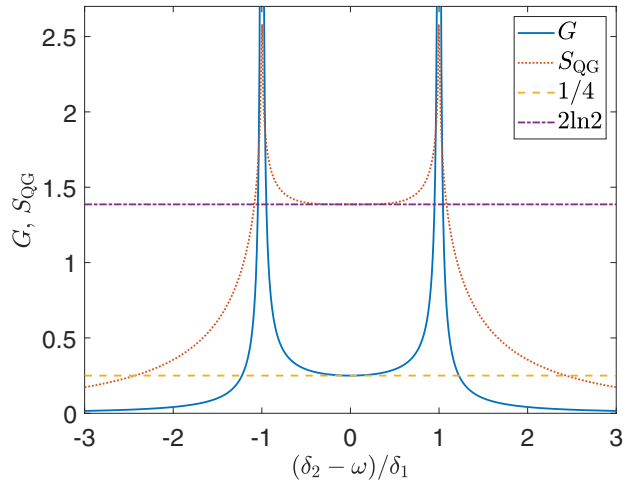


FIG. 1. Integrated QMT G (solid line) and GEE S_{QG} (dotted line) of the harmonically driven spin chain. The numbers of unit cells and filled single-particle states are $L = N = 1000$ (half-filling). The subsystem size is $L_A = 500$ (equal bipartition). The horizontal dashed and dashed-dotted lines highlight the values of G and S_{QG} in the topological limit $\omega = \delta_2$, respectively.

is uniformly filled by fermions, with one at each k in the first BZ. Plugging Eq. (20) into (E4), diagonalizing the overlap matrices O^A and O^{A_0} for a given subsystem size L_A , and inserting their spectrum into Eqs. (9) and (7), we finally arrive at the von Neumann EE and GEE following Eq. (5). For any given subsystem size $L_A \leq L$ and particle number $N \leq L$, we could then analyze the scaling properties of EE and its behaviors around phase transition points in our Floquet system.

In Fig. 2, we present typical scaling behaviors of EE and GEE vs the size L_A of subsystem A . First, we notice that in either the topological ($|\mu| < 1$) or trivial ($|\mu| > 1$) phase, the S_{QG} will converge to a finite value that is independent of L_A for the system at half-filling [Fig. 2(a)] or other possible filling fractions [Figs. 2(c) and 2(d)]. Therefore, the GEE tends to follow an area-law scaling vs the subsystem size at any filling fractions, so long as the two Floquet bands of the system are well separated by quasienergy gaps. The quantum geometric origin of GEE thus endows it with certain robustness to the change of particle numbers in the system regarding its scaling properties. Second, at the topological transition points [$\mu = \pm 1$ in Fig. 2(b)], we have $S_{\text{QG}} \propto \ln[\sin(\pi L_A/L)]$. It suggests that the GEE at half-filling scales logarithmically versus the subsystem size in these situations (with gapless quasienergy bands), which is expected for 1D critical metallic phases. Third, in all the considered cases, we find $S_{A_0} = 0$ when $N = L$. Therefore, the bipartite EE of our system at half-filling is solely originated from the quantum geometry of Floquet-Bloch states in k space. This conclusion should hold in both Floquet and static systems. Finally, the saturation value of S_{QG} increases monotonically when the system approaches its topological phase transition point from either side of the parameter space [see Figs. 1 and 2(a)]. As will be demonstrated below, the scaling laws and critical properties of GEE found here are generic and not restricted to the driven spin chain model considered in this section. Moreover, richer patterns in QMT and GEE could be identified when the system

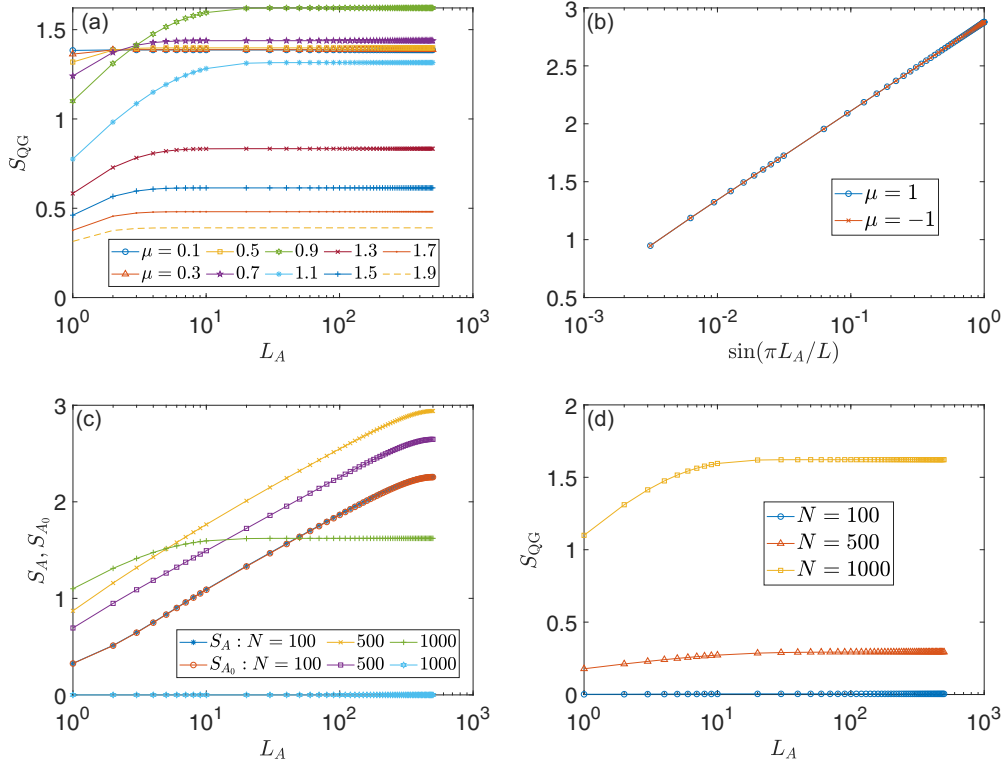


FIG. 2. EE of the harmonically driven spin chain vs the subsystem size L_A under PBC. (a) GEE at half-filling ($N = L$) vs L_A , with different values of $\mu = (\delta_2 - \omega)/\delta_1$ for different curves as shown in the figure legend. (b) GEE at half-filling ($N = L$) vs L_A for $\mu = \pm 1$. (c) The total and nongeometric parts of EE, S_A , and S_{A_0} vs L_A at different filling fractions N/L , with $L = 1000$ and $\mu = 0.9$. (d) GEE vs L_A at different filling fractions N/L , with $L = 1000$ and $\mu = 0.9$. The numbers of filled Floquet single-particle states N for different curves are shown in the legends of (c) and (d).

possesses multiple Floquet topological phases and phase transitions, as will be considered in the following sections.

IV. ON-RESONANCE DOUBLE KICKED ROTOR: QMT AND GEE

In the last section, the driven spin chain we introduced owns two Floquet phases with distinct topological properties. In this section, we investigate the QMT and GEE of a 1D Floquet insulator with richer topological phases and transitions [71–73]. Following Ref. [71], we consider the lattice version of an on-resonance double kicked rotor (ORDKR), which forms a paradigmatic platform in the study of dynamical localization, quantum chaos, and Floquet topological matter [10]. The lattice Hamiltonian of such an ORDKR takes the form [71]

$$\hat{H}(t) = V(t) \sum_n n^2 \hat{c}_n^\dagger \hat{c}_n + \frac{1}{2} \sum_n [J(t) \hat{c}_n^\dagger \hat{c}_{n+1} + \text{H.c.}] \quad (21)$$

Here $n \in \mathbb{Z}$ is the lattice index and \hat{c}_n^\dagger creates a fermion on the lattice site n . The onsite potential $V(t)$ and nearest-neighbor hopping amplitude $J(t)$ have the expressions

$$[V(t), J(t)] = \begin{cases} (0, iK_1), & t \in [\ell T, \ell T + T/4) \\ (V, 0), & t \in [\ell T + T/4, \ell T + T/2) \\ (0, K_2), & t \in [\ell T + T/2, \ell T + 3T/4) \\ (-V, 0), & t \in [\ell T + 3T/4, \ell T + T) \end{cases} \quad (22)$$

where $K_1, K_2, V \in \mathbb{R}$, $\ell \in \mathbb{Z}$, and T is the driving period. In the following calculations, we choose $4\hbar/T$ as the unit of energy and set $V = \pi/2$ in order to obtain a two-band model. It is clear that the $\hat{H}(t)$ in Eq. (21) does not have any spatial periodicity. However, the Floquet operator of the system that governs its evolution over a complete driving period (e.g., from $t = 5T/8$ to $T + 5T/8$) takes the form

$$\begin{aligned} \hat{U} &= e^{-\frac{i}{4} \sum_n K_2 (\hat{c}_n^\dagger \hat{c}_{n+1} + \text{H.c.})} \\ &\times e^{-\frac{i}{2} \pi \sum_n n^2 \hat{c}_n^\dagger \hat{c}_n} e^{-\frac{i}{2} \sum_n iK_1 (\hat{c}_n^\dagger \hat{c}_{n+1} - \text{H.c.})} \\ &\times e^{\frac{i}{2} \pi \sum_n n^2 \hat{c}_n^\dagger \hat{c}_n} e^{-\frac{i}{4} \sum_n K_2 (\hat{c}_n^\dagger \hat{c}_{n+1} + \text{H.c.})}, \end{aligned} \quad (23)$$

which has the spatial periodicity under the translation over two lattice sites ($n \rightarrow n + 2$). Performing the Fourier transformation from position to momentum representations, we can express the Floquet operator of the system as $\hat{U} = \sum_k \hat{\Psi}_k^\dagger U(k) \hat{\Psi}_k$, where $\hat{\Psi}_k^\dagger = (\hat{c}_{k,a}^\dagger, \hat{c}_{k,b}^\dagger)$ collects creation operators on odd and even sites within each unit cell and k is the quasimomentum. The Floquet matrix $U(k)$ is given by [71]

$$\begin{aligned} U(k) &= e^{-\frac{i}{2} K_2 [\cos(k/2)\sigma_x + \sin(k/2)\sigma_y]} \\ &\times e^{-iK_1 [\sin(k/2)\sigma_x - \cos(k/2)\sigma_y]} \\ &\times e^{-\frac{i}{2} K_2 [\cos(k/2)\sigma_x + \sin(k/2)\sigma_y]}, \end{aligned} \quad (24)$$

where

$$\mathcal{K}_1 \equiv K_1 \sin(k/2), \quad \mathcal{K}_2 \equiv K_2 \cos(k/2), \quad (25)$$

and $\sigma_{x,y}$ are Pauli matrices acting on sublattice degrees of freedom. Applying the Taylor expansion to each exponential term in $U(k)$, we find

$$U(k) = \cos \mathcal{K}_1 \cos \mathcal{K}_2 - i(h_x \sigma_x + h_y \sigma_y), \quad (26)$$

where

$$\begin{aligned} h_x &= \cos \frac{k}{2} \cos \mathcal{K}_1 \sin \mathcal{K}_2 + \sin \frac{k}{2} \sin \mathcal{K}_1, \\ h_y &= \sin \frac{k}{2} \cos \mathcal{K}_1 \sin \mathcal{K}_2 - \cos \frac{k}{2} \sin \mathcal{K}_1. \end{aligned} \quad (27)$$

The quasienergy spectrum of our system thus contains two Floquet bands under the PBC with dispersion relations $E_{\pm}(k) = \pm \arccos(\cos \mathcal{K}_1 \cos \mathcal{K}_2)$. These two bands could touch with each other at the center or boundary of the first quasienergy BZ $E_{\pm} \in [-\pi, \pi)$, leading to the gap-closing conditions $\cos \mathcal{K}_1 \cos \mathcal{K}_2 = 1$ and -1 at the zero and π quasienergies, respectively. The boundary curves between different Floquet topological insulating phases can further be found as [71]

$$\frac{\nu^2 \pi^2}{K_1^2} + \frac{\mu^2 \pi^2}{K_2^2} = 1, \quad \nu, \mu \in \mathbb{Z}. \quad (28)$$

When K_1 or K_2 is swept across a phase boundary, the topological invariants of ORDKR will get quantized changes, which are associated with the variation of degenerate Floquet zero and π edge modes in the system under the open boundary condition [71].

The Floquet eigenstates of $U(k)$ are obtained by solving the eigenvalue equation $U(k)|\psi_{\pm}(k)\rangle = e^{-iE_{\pm}(k)}|\psi_{\pm}(k)\rangle$. As $U(k)$ and the term $h_x \sigma_x + h_y \sigma_y$ in Eq. (26) commute, they share the same eigenbasis. We could then focus on the eigenstates of $h_x \sigma_x + h_y \sigma_y$ in Eq. (26) in order to reveal the quantum geometry and geometric EE of ORDKR.

To obtain the QMT of ORDKR, we plug Eqs. (25) and (27) and $E = \sqrt{h_x^2 + h_y^2}$ into Eq. (B6). Integrating the resulting $g_{kk} = g_{kk}^{xy}$ over the first BZ yields the integrated QMT of a filled Floquet quasienergy band, i.e., $G = \int_{-\pi}^{\pi} \frac{dk}{2\pi} g_{kk}$. In Fig. 3, we present G vs the kicking strength K_1 with $K_2 = 0.5\pi$. According to Eq. (28), the quasienergy gap between two Floquet bands of the system closes when $K_1 = \nu\pi$ for $\nu \in \mathbb{Z}$ in this case. We observe that the integrated QMT becomes diverge at these transition points. This is true for other combinations of system parameters satisfying Eq. (28). Notably, the divergent behaviors in G appear when the Floquet bands touch at either the quasienergy zero (with $K_1 = 2\nu\pi$) or π [with $K_1 = (2\nu - 1)\pi$]. Therefore, the QMT could show nonanalytic signatures when the ORDKR undergoes both normal and anomalous topological transitions between different Floquet phases, offering a quantum geometric probe to these nonequilibrium phase transitions. To find the GEE, we first obtain the overlap between any two Floquet eigenstates in the lower quasienergy band, i.e., $\mathcal{O}_{-}^{xy}(k, k')$, according to Eq. (A6), where $E = \sqrt{h_x^2 + h_y^2}$ and the h_x, h_y are given by Eq. (27). Replacing the $\langle \psi_k | \psi_{k'} \rangle$ in Eq. (E4) by $\mathcal{O}_{-}^{xy}(k, k')$ and following the recipes in Appendixes C–E, we can obtain the total EE together with its geometric and nongeometric parts from the eigenspectrum of overlap matrix O^A in k space.

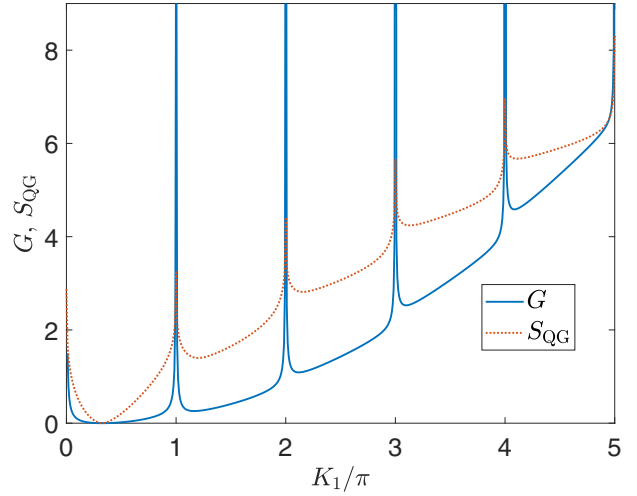


FIG. 3. Integrated QMT G (solid line) and GEE S_{QG} (dotted line) of the on-resonance double kicked rotor. The kicking strength is $K_2 = 0.5\pi$. The numbers of unit cells and filled single-particle states are $L = N = 1000$ (half-filling). The subsystem size is $L_A = 500$ (equal bipartition). Topological phase transitions happen at $K_1 = \nu\pi$ [Eq. (28)] for $\nu \in \mathbb{Z}$.

The GEE versus K_1 at half-filling and under equal bipartition for the ORDKR is shown in Fig. 3. We find that around each topological transition point, the GEE shows a cusp, with a discontinuous derivative vs K_1 at different sides of $K_1 = \nu\pi$. Away from the topological transition points, the amount of GEE increases gradually with the increase of K_1 . This is related to the raise of topological edge-state numbers at zero and π quasienergies following the increase of kicking strengths in ORDKR [71]. These Floquet edge modes yield gradually increased contributions to GEE across the entanglement cuts when a bipartition is taken in the bulk. Putting together, thanks to the close integration among quantum information, geometry, and topology, we could employ the GEE as an additional probe to the phases and transitions in 1D Floquet topological insulators with large topological invariants.

To further decode the scaling laws of EE, we could first decompose the system S into two complementary parts as $S = A \cup \bar{A}$. The behaviors of EE vs the subsystem size L_A and the filling fraction N/L of a Floquet band can then be worked out, with N the total number of particles and $L = L_A + L_{\bar{A}}$ the system size. Results of EE for typical cases of the ORDKR are shown in Fig. 4, which are obtained following the procedure in Appendixes C–E. First, we notice that when the system at half-filling resides in gapped Floquet topological insulator phases [the cases in Fig. 4(a)], the GEE would always converge to an area-law scaling vs the system size with the increase of L_A . In contrast, when the two Floquet bands meet at the quasienergy zero or π [the cases in Fig. 4(b)], the system becomes critical at half-filling and the GEE follows a log-law scaling vs L_A . These different scaling laws (area law and log law) of GEE are generic when the ORDKR is prepared in other gapped and gapless Floquet topological phases, respectively. A further comparison between the results in Figs. 4(c) and 4(d) suggests

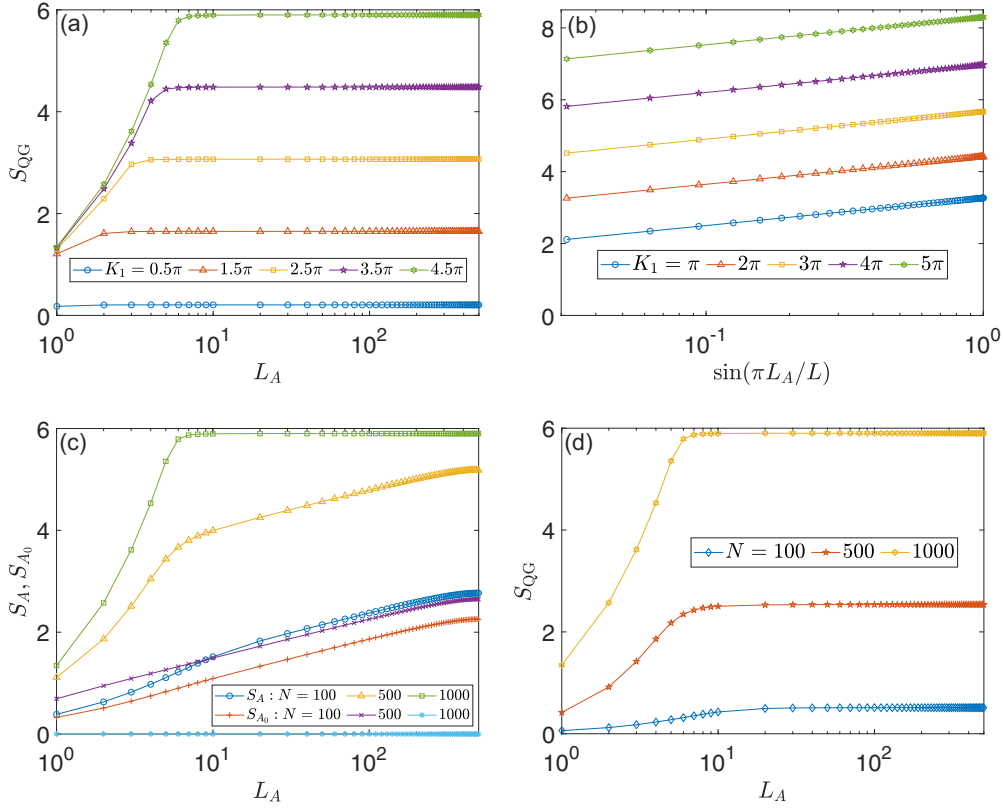


FIG. 4. EE of the on-resonance double kicked rotor vs the subsystem size L_A under PBC, with $K_2 = 0.5\pi$ for all panels. (a) GEE at half-filling ($N = L$) vs L_A , with different values of K_1 for different curves as shown in the figure legend. (b) GEE at half-filling ($N = L$) vs L_A for $K_1 = \pi, 2\pi, 3\pi, 4\pi$. (c) The total and nongeometric parts of EE, S_A , and S_{A_0} vs L_A at different filling fractions N/L , with $L = 1000$ and $K_1 = 4.5\pi$. (d) GEE vs L_A at different filling fractions N/L , with $L = 1000$ and $K_1 = 4.5\pi$. The numbers of filled Floquet single-particle states N for different curves are shown in the legends of (c) and (d).

that the bipartite EE of ORDKR is fully quantum geometric if the many-particle state of the system uniformly fills a Floquet band. That is, the nongeometric EE S_{A_0} vanishes and the total EE S_A becomes equal to S_{QG} at half-filling [$N/L = 1$ in Figs. 4(c) and 4(d)]. This observation clarifies the geometric origin of EE in 1D Floquet topological insulators, i.e., the bipartite EE of a filled Floquet band is uniquely determined by the quantum geometry of the populated Floquet-Bloch eigenstates. Finally, even though both the bipartite EE and its nongeometric part could vary with the subsystem size L_A , the GEE always satisfies an area law versus the subsystem size. This is true regardless of the filling fraction ($N/L \in (0, 1)$) of the considered Floquet band, so long as it is gapped from the other bands. The scaling behavior of GEE may thus be robust to the variations of Floquet-band populations through certain dynamical processes, which further highlights its geometric origin.

In comparison with the driven spin chain studied in the last section, the QMT and GEE found here show quantitatively richer patterns due to the underlying multiple Floquet topological insulating phases and transitions within the ORDKR. Meanwhile, the generic scaling and critical properties of QMT and EE in these two models are coincident. These general relations will hold also in 1D Floquet topological superconductors, as will be unveiled in the following section.

V. PERIODICALLY QUENCHED KITAEV CHAIN: QMT AND GEE

We now consider the quantum geometry and geometric EE of Floquet states in a periodically quenched Kitaev chain (PQKC) [74,75], whose time-dependent Hamiltonian takes the form

$$\hat{H}(t) = \begin{cases} \hat{H}_1, & t \in [\ell T, \ell T + T/4) \\ \hat{H}_2, & t \in [\ell T + T/4, \ell T + 3T/4) \\ \hat{H}_1, & t \in [\ell T + 3T/4, \ell T + T). \end{cases} \quad (29)$$

Here $\ell \in \mathbb{Z}$ counts the number of driving period T . The piecewise Hamiltonians

$$\hat{H}_1 = \frac{1}{2} \sum_n \Delta(\hat{c}_n \hat{c}_{n+1} + \text{H.c.}), \quad (30)$$

$$\hat{H}_2 = \frac{1}{2} \sum_n [\mu(\hat{c}_n^\dagger \hat{c}_n - 1/2) + J\hat{c}_n^\dagger \hat{c}_{n+1} + \text{H.c.}], \quad (31)$$

where \hat{c}_n^\dagger creates a fermion on the lattice site $n \in \mathbb{Z}$. Δ is the superconducting pairing strength, μ is the chemical potential, and J is the nearest-neighbor hopping amplitude. The Floquet operator of the system, which leads its evolution over a complete driving period (e.g., from $t = \ell T + 0^-$ to $t = \ell T + T + 0^-$) takes the form of $\hat{U} = e^{-i\frac{T}{4n}\hat{H}_1} e^{-i\frac{T}{2n}\hat{H}_2} e^{-i\frac{T}{4n}\hat{H}_1}$. Under the PBC, we can transform \hat{U} from the position to momentum

representations and express it in terms of the Nambu spinor basis as $\hat{U} = \sum_k \hat{\mathcal{E}}_k^\dagger U(k) \hat{\mathcal{E}}_k$, where k is the Bloch quasimomentum and $\hat{\mathcal{E}}_k^\dagger = (\hat{c}_k^\dagger, \hat{c}_{-k})$. The Floquet operator $U(k)$ in k space reads as

$$U(k) = e^{-\frac{i}{2}d_y\sigma_y} e^{-id_z\sigma_z} e^{-\frac{i}{2}d_y\sigma_y}, \quad (32)$$

where $\sigma_{y,z}$ are Pauli matrices,

$$d_y = \Delta \sin k, \quad d_z = \mu + J \cos k, \quad (33)$$

and we have set $2\hbar/T$ as the unit of energy. Applying the Taylor expansion to each exponential term of $U(k)$ and recombining the relevant terms, we find

$$U(k) = \cos d_y \cos d_z - i(h_y\sigma_y + h_z\sigma_z), \quad (34)$$

$$h_y = \sin d_y \cos d_z, \quad h_z = \sin d_z. \quad (35)$$

The Floquet operator $U(k)$ has two quasienergy bands, whose dispersions are $E_\pm(k) = \pm \arccos(\cos d_y \cos d_z)$. The quasienergy spectrum of $U(k)$ then becomes gapless when $\cos d_y \cos d_z = \pm 1$, yielding the borderlines between its different Floquet topological phases as [75]

$$\frac{\kappa^2\pi^2}{\Delta^2} + \frac{(\nu\pi - \mu)^2}{J^2} = 1, \quad \kappa, \nu \in \mathbb{Z}. \quad (36)$$

Meanwhile, we notice that the matrix $h(k) \equiv h_y\sigma_y + h_z\sigma_z$ in Eq. (34) commutes with the Floquet operator $U(k)$. They thus share the same Floquet eigenstates. This allows us to deduce the QMT and GEE of our PQKC model from the eigenbasis of $h(k)$.

Plugging Eqs. (33) and (35) into (B8), we can find the QMT of our system analytically as

$$g_{kk} = \frac{[J \sin k \sin d_y + (\Delta/2) \cos k \cos d_y \sin(2d_z)]^2}{4(\sin^2 d_y \cos^2 d_z + \sin^2 d_z)^2}. \quad (37)$$

The integrated contribution of g_{kk} over the first BZ, i.e., $G = \int_{-\pi}^{\pi} \frac{dk}{2\pi} g_{kk}$ can be further obtained numerically. In Fig. 5, we present G vs the hopping amplitude J for a typical set of system parameters. We find that the QMT becomes divergent at every topological phase transition point in the system, where the gap between $E_\pm(k)$ closes at the quasienergy zero (with $J = 2\nu\pi \pm \pi/4$ and $\nu \in \mathbb{Z}$) or π [with $J = (2\nu - 1)\pi \pm \pi/4$ and $\nu \in \mathbb{Z}$]. Therefore, both the normal and anomalous topological transitions between different Floquet superconducting phases could yield nonanalytic signatures in the QMT of a filled Floquet band. The latter could thus supply a quantum geometric probe to the phase transitions in Floquet topological superconductors.

To find out the GEE, we could first insert Eq. (35) and $E(k) = \sqrt{h_y^2 + h_z^2}$ into Eq. (A8), yielding the overlap $\mathcal{O}_-^{yz}(k, k')$ between eigenstates in the lower Floquet band with quasienergy dispersion $E_-(k)$. Replacing the term $\langle \psi_k | \psi_{k'} \rangle$ with $\mathcal{O}_-^{yz}(k, k')$ in Eq. (E4) gives us the wave-function overlap $\mathcal{O}_{k,k'}^A$, from which the total, nongeometric and geometric parts of EE could be deduced following Appendixes D and E. The dotted line in Fig. 5 shows the change of GEE with respect to J for the PQKC at half-filling and under equal bipartition. We find that the amount of S_{QG} gradually raises with the increase of J , and at each topological transition point it exhibits a cusp structure. The former is related to the fact that the topological

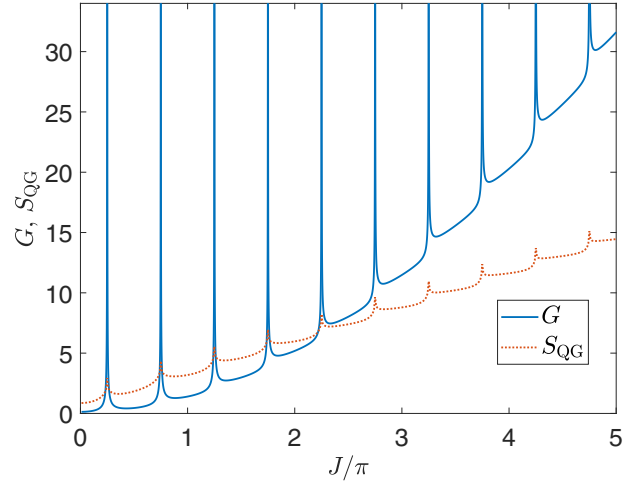


FIG. 5. Integrated QMT G (solid line) and GEE S_{QG} (dotted line) of the periodically quenched Kitaev chain. Other system parameters are $\Delta = \pi/2$ and $\mu = \pi/4$. The numbers of unit cells and filled single-particle states are $L = N = 1000$ (half-filling). The subsystem size is $L_A = 500$ (equal bipartition). Topological phase transitions happen at $J = \pi/4 + \nu\pi/2$ for $\nu \in \mathbb{Z}$ [Eq. (36)].

invariants of PQKC could increase monotonically following a sequence of topological transitions triggered by the increase of J , generating more and more Floquet Majorana edge modes at zero and π quasienergies that could contribute to EE when a bipartition is taken in the bulk [75]. This is in stark contrast to the results shown in Fig. 1, where the system only possesses two different topological phases. The observed cusps in S_{QG} further imply that one can use GEE as a detector for the topological transitions between distinct Floquet superconducting phases from an integrated view of quantum geometry and information.

To further decode the scaling properties of EE in our PQKC, we present in Fig. 6 the total, geometric, and nongeometric parts of EE vs the subsystem size L_A for some typical cases, both away from and at topological transition points. The calculations of EE also follow the Appendixes D and E. In Fig. 6(a), we observe that in gapped Floquet superconducting phases, the S_{QG} will finally converge to a value for each case that is increasing with J but independent of L_A . Therefore, the S_{QG} at half-filling follows an area-law scaling vs the system size. A further comparison between Figs. 6(c) and 6(d) suggests that this area-law scaling behavior is independent of the filling fraction N/L of the considered Floquet band. Therefore, in topological phases with gapped Floquet bands, the GEE of PQKC follows an area law regardless of the filling fraction of the band. This is consistent with our results in Secs. III and IV for other Floquet models. Next, we notice that the GEE follows subvolume log-law scalings at the critical points between different Floquet superconducting phases, as shown in Fig. 6(b). This is true regardless of whether the Floquet bands close their respective gaps at the center ($E = 0$) or boundary ($E = \pi$) of the first quasienergy BZ. Referring to the results in Figs. 2(b) and 4(b), we find that the log-law scalings of GEE at topological transition points of 1D Floquet phases can be satisfied in general. Third, away from the half-filling, both the total and nongeometric parts of EE are

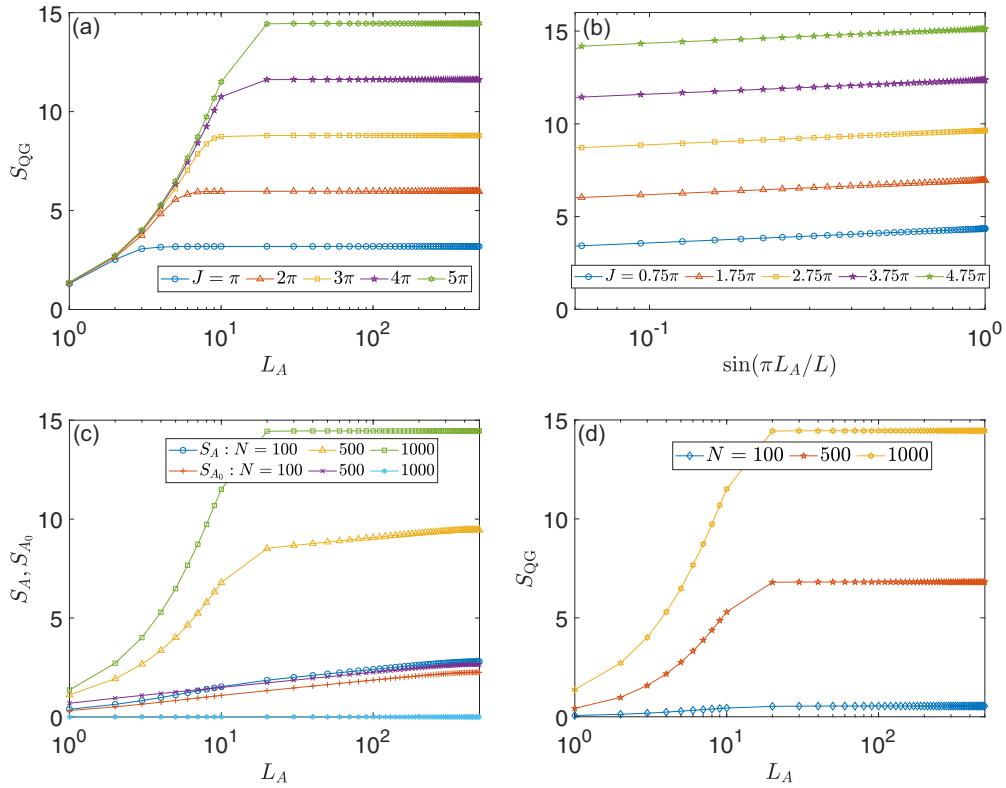


FIG. 6. EE of the periodically quenched Kitaev chain vs the subsystem size L_A under PBC. Other system parameters are $\Delta = \pi/2$ and $\mu = \pi/4$ for all panels. (a) GEE at half-filling ($N = L$) vs L_A , with different values of J for different curves as shown in the figure legend. (b) GEE at half-filling ($N = L$) vs L_A for $J = 0.75\pi + \nu\pi$ and $\nu = 0, 1, 2, 3, 4$. (c) The total and nongeometric parts of EE, S_A , and S_{A_0} vs L_A at different filling fractions N/L , with $L = 1000$ and $J = 5\pi$. (d) GEE vs L_A at different filling fractions N/L , with $L = 1000$ and $J = 5\pi$. The numbers of filled Floquet single-particle states N for different curves are shown in the legends of (c) and (d).

sensitive to the change of subsystem size L_A , as shown in Fig. 6(c). However, at half-filling, the nongeometric EE S_{A_0} vanishes, and the total EE becomes fully quantum geometric, as observable from the curves with $N = L$ in Figs. 6(c) and 6(d). This is also coincident with our results for the harmonically driven spin chain and double kicked rotor in the last two sections. Therefore, the bipartite EE for states filling a gapped quasienergy band tends out to be solely of quantum geometric origin and satisfies an area-law scaling in 1D Floquet systems. Physical properties associated with such GEE should then be robust to certain dynamical variations of the system, yielding auxiliary probes to the topological phase transitions in 1D Floquet superconducting systems.

VI. SUMMARY AND DISCUSSION

In this work, we revealed the quantum geometry and geometric entanglement entropy of typical Floquet topological phases in 1D systems. Based on the detailed calculations of quantum geometric tensors, entanglement entropy and their scaling behaviors for periodically driven spin chains, Floquet topological insulators, and superconductors, we could arrive at the following general conclusions.

First, for a uniformly filled Floquet quasienergy band, the quantum metric tensor integrated over the occupied Floquet-state manifold becomes divergent at the transition points between different Floquet topological phases. The quantum

geometry of Floquet-Bloch states could thus offer an efficient means to probe topological phase transitions in Floquet systems. Second, regardless of the filling fractions of a gapped Floquet-Bloch band, the geometric EE as considered in this study always follows an area-law scaling vs the system size. This observation implies certain levels of robustness of the geometric EE to the variation of Floquet band populations, which may find applications in the characterization of quasienergy bands in particle-number nonconserved (or open-system) situations. Third, for a Floquet band at unit filling, the bipartite EE becomes purely quantum geometric. The EE of Floquet systems at half-filling, as considered in previous studies [37], could thus be viewed as geometric EE, which might be insensitive to the changes of some dynamical details of the system. Finally, the bipartite geometric EE of a filled Floquet-Bloch band shows a critical log-law scaling versus the system size at each topological phase transition point. Close to the transition point, the geometric EE further exhibits the shape of a cusp versus the transition-driven parameter of the system. These observations suggest that the geometric EE could provide us with an efficient probe to identify Floquet topological phase transitions from a hybrid perspective of quantum geometry and quantum information.

As an additional comment, for all the models we considered, the two Floquet bands can be separated by two gaps at both the quasienergies zero and π , instead of a single gap around zero energy in nondriven two-band models. Both

the zero and π Floquet gaps can be topologically nontrivial and admit degenerate topological edge modes under the open boundary condition [71,75]. The two Floquet bands could further touch with each other at either the quasienergy zero or π , causing two possible avenues of topological phase transitions. When the Floquet bands meet and reseparate at the quasienergy π , an anomalous phase transition that cannot manifest in a static two-band system could happen, whose signatures in quantum geometry and GEE are unique to Floquet systems and are characterized in detail through our model studies.

The conclusions as mentioned above are expected to be generic and not restricted to the models considered in this work. The verification (and possible extension) of these results for Floquet systems in other symmetry classes and in higher spatial dimensions deserves further considerations. The properties of Floquet quantum geometry, geometric EE, and their robustness against more complicated effects such as disorders and interactions constitute interesting directions of future research. Besides, the experimental detection of quantum metric tensor and geometric EE of Floquet states could be within reach in various quantum simulators like nitrogen-vacancy center in diamonds [76,77], superconducting qubits [78,79], and ultracold atoms [80–82].

ACKNOWLEDGMENTS

This work is supported by the Fundamental Research Funds for the Central Universities (Grant No. 202364008), the National Natural Science Foundation of China (Grants No. 12275260, No. 12047503, and No. 11905211), and the Young Talents Project of Ocean University of China.

APPENDIX A: WAVE-FUNCTION OVERLAP OF 1D, TWO-BAND FLOQUET EFFECTIVE HAMILTONIANS

In this Appendix, we compute the overlap between eigenstates within a single Floquet-Bloch band for 1D lattice

models. Under time-periodic drivings and spatial periodic boundary conditions (PBCs), the Hamiltonian of such a lattice model takes the form $\hat{H}(t) = \sum_k |k\rangle H(k, t) \langle k|$, where $k \in [-\pi, \pi)$ is the quasimomentum. The Floquet operator of the system then reads as $\hat{U} = \sum_k |k\rangle U(k) \langle k|$, where $U(k) \equiv \hat{T} e^{-i \int_0^T H(k, t') dt'}$ with T being the driving period. Formally, one can write $U(k)$ as $U(k) = e^{-iH(k)}$, with the effective Floquet-Bloch Hamiltonian $H(k)$ defined by $H(k) = i \ln U(k)$. For a generic 1D lattice with two internal degrees of freedom (spins, sublattices, etc.) in each unit cell, one can always express the Floquet effective Hamiltonian $H(k)$ as

$$H(k) = h_0(k)\sigma_0 + h_x(k)\sigma_x + h_y(k)\sigma_y + h_z(k)\sigma_z. \quad (\text{A1})$$

Here σ_0 is the 2×2 identity matrix. σ_x , σ_y , and σ_z are Pauli matrices. $h_0(k)$, $h_x(k)$, $h_y(k)$, and $h_z(k)$ can be real functions of k . By definition, the $H(k)$ here incorporates the all-around information of the system's stroboscopic dynamics over each complete driving period. Its quasienergy spectrum could thus be significantly different from and more complicated than the nondriven counterpart of the system. By diagonalizing $H(k)$, the dispersion relations of its two Floquet bands (defined modulus 2π and indexed by s) are found to be

$$E_s(k) = h_0(k) + sE(k), \quad s = \pm \quad (\text{A2})$$

where

$$E(k) = \sqrt{h_x^2(k) + h_y^2(k) + h_z^2(k)}. \quad (\text{A3})$$

The associated Floquet eigenstates of $H(k)$ are further given by

$$|\psi_s(k)\rangle = \frac{1}{\sqrt{2E(k)[E(k) + sh_z(k)]}} \begin{pmatrix} h_z(k) + sE(k) \\ h_x(k) + ih_y(k) \end{pmatrix}, \quad (\text{A4})$$

where $s = \pm$. For any two eigenstates $|\psi_s(k)\rangle$ and $|\psi_{s'}(k')\rangle$ of $H(k)$ in the same Floquet band, their overlap reads as

$$\mathcal{O}_s(k, k') \equiv \langle \psi_s(k) | \psi_{s'}(k') \rangle = \frac{[h_x(k) - ih_y(k)][h_x(k') + ih_y(k')] + [E(k) + sh_z(k)][E(k') + sh_z(k')]}{2\sqrt{E(k)E(k')}[E(k) + sh_z(k)][E(k') + sh_z(k')]} \quad (\text{A5})$$

If $H(k)$ has the chiral symmetry $\mathcal{S} = \sigma_z$, such that $\sigma_z H(k) \sigma_z = -H(k)$, we would have $h_0(k) = h_z(k) = 0$ in Eq. (A1), and the overlap $\mathcal{O}_s(k, k')$ in Eq. (A5) reduces to

$$\mathcal{O}_s^{xy}(k, k') = \frac{1}{2} + \frac{[h_x(k) - ih_y(k)][h_x(k') + ih_y(k')]}{2E(k)E(k')}. \quad (\text{A6})$$

If $H(k)$ has the chiral symmetry $\mathcal{S} = \sigma_y$, such that $\sigma_y H(k) \sigma_y = -H(k)$, we would have $h_0(k) = h_y(k) = 0$ in Eq. (A1), and the overlap $\mathcal{O}_s(k, k')$ in Eq. (A5) reduces to

$$\mathcal{O}_s^{zx}(k, k') = \frac{h_x(k)h_x(k') + [E(k) + sh_z(k)][E(k') + sh_z(k')]}{2\sqrt{E(k)E(k')}[E(k) + sh_z(k)][E(k') + sh_z(k')]} \quad (\text{A7})$$

Finally, when $H(k)$ has the chiral symmetry $\mathcal{S} = \sigma_x$ so that $\sigma_x H(k) \sigma_x = -H(k)$, we will have $h_0(k) = h_x(k) = 0$ in

Eq. (A1), and the overlap $\mathcal{O}_s(k, k')$ in Eq. (A5) becomes

$$\mathcal{O}_s^{yz}(k, k') = \frac{h_y(k)h_y(k') + [E(k) + sh_z(k)][E(k') + sh_z(k')]}{2\sqrt{E(k)E(k')}[E(k) + sh_z(k)][E(k') + sh_z(k')]} \quad (\text{A8})$$

Equations (A6)–(A8) will be used in the calculations of quantum metric tensor and geometric entanglement entropy for our 1D Floquet systems in the main text.

APPENDIX B: QMT OF 1D, TWO-BAND HAMILTONIANS

In this Appendix, we deduce the quantum metric tensor of Floquet-Bloch bands for 1D driven lattice models, with a focus on two-band settings. For a 1D system described by the Floquet-Bloch effective Hamiltonian in Eq. (A1), the quantum

metric tensor [51] in k space has a single component, i.e.,

$$\begin{aligned} g_{kk}^s &= \langle \partial_k \psi_s | \partial_k \psi_s \rangle - \langle \partial_k \psi_s | \psi_s \rangle \langle \psi_s | \partial_k \psi_s \rangle \\ &= \langle \partial_k \psi_s | \psi_{-s} \rangle \langle \psi_{-s} | \partial_k \psi_s \rangle. \end{aligned} \quad (\text{B1})$$

Here, $|\psi_s\rangle = |\psi_s(k)\rangle$ is given by Eq. (A4) and $s = \pm$ label the two Floquet bands. According to Eq. (A3), we could obtain

$$\partial_k E(k) = \sum_{w=x,y,z} \frac{h_w(k) \partial_k h_w(k)}{E(k)} \quad (\text{B2})$$

$$\langle \psi_{-s} | \partial_k \psi_s \rangle = \frac{s[h_x(h_z \partial_k h_x - h_x \partial_k h_z) - h_y(h_y \partial_k h_z - h_z \partial_k h_y)] + iE(h_x \partial_k h_y - h_y \partial_k h_x)}{2E^2 \sqrt{(E + h_z)(E - h_z)}}. \quad (\text{B4})$$

Therefore, according to Eq. (B1), the QMT reads as

$$g_{kk} = g_{kk}^s = \frac{[h_x(h_z \partial_k h_x - h_x \partial_k h_z) - h_y(h_y \partial_k h_z - h_z \partial_k h_y)]^2 + E^2(h_x \partial_k h_y - h_y \partial_k h_x)^2}{4E^4(E + h_z)(E - h_z)}. \quad (\text{B5})$$

It is clear that the g_{kk} as obtained in Eq. (B5) is independent of the Floquet band index s .

Referring to the Appendix A, we have $h_z(k) = 0$ for a chiral symmetric $H(k)$ with $\mathcal{S} = \sigma_z$. The related g_{kk} then reduces to

$$g_{kk}^{xy} = \frac{[h_x(k) \partial_k h_y(k) - h_y(k) \partial_k h_x(k)]^2}{4E^4(k)}. \quad (\text{B6})$$

Similarly, for a chiral symmetric $H(k)$ with $\mathcal{S} = \sigma_y$, we have $h_y(k) = 0$ and the g_{kk} reduces

$$g_{kk}^{zx} = \frac{[h_z(k) \partial_k h_x(k) - h_x(k) \partial_k h_z(k)]^2}{4E^4(k)}. \quad (\text{B7})$$

Meanwhile, for an $H(k)$ with the chiral symmetry $\mathcal{S} = \sigma_x$, we have $h_x(k) = 0$ and the resulting QMT reads as

$$g_{kk}^{yz} = \frac{[h_y(k) \partial_k h_z(k) - h_z(k) \partial_k h_y(k)]^2}{4E^4(k)}. \quad (\text{B8})$$

Note in passing that in all the cases we have $g_{kk} \geq 0$, as expected. With the help of Eqs. (B6)–(B8), we could further work out the integration of QMT for the different Floquet models considered in the main text.

For 1D chiral symmetric models, a connection between the QMT and the topological winding number could be identified. Let us denote the effective Floquet-Bloch Hamiltonian of such a system as $H_{ab}(k) = h_a(k)\sigma_a + h_b(k)\sigma_b$, where $a, b = x, y, z$ and $a \neq b$. The chiral symmetry operator of $H_{ab}(k)$ is thus the Pauli matrix σ_c with $c = x, y, z$ and $c \neq a, b$. The topological phases of the system described by $H_{ab}(k)$ can be characterized by the integer winding number

$$w = \int_{-\pi}^{\pi} \frac{dk}{2\pi} \partial_k \phi^{ab}(k), \quad (\text{B9})$$

where the winding angle $\phi^{ab}(k) \equiv \arctan[h_b(k)/h_a(k)]$, and thus

$$\partial_k \phi^{ab}(k) = \frac{h_a(k) \partial_k h_b(k) - h_b(k) \partial_k h_a(k)}{E^2(k)}, \quad (\text{B10})$$

and

$$\partial_k \frac{1}{E(k)} = - \sum_{w=x,y,z} \frac{h_w(k) \partial_k h_w(k)}{E^3(k)}. \quad (\text{B3})$$

Using these relations together with Eq. (A4), we find after straightforward calculations that

with $E^2(k) = h_a^2(k) + h_b^2(k)$. According to Eqs. (B6)–(B8), the QMT of such a system reads as

$$g_{kk}^{ab} = \frac{[h_a(k) \partial_k h_b(k) - h_b(k) \partial_k h_a(k)]^2}{4E^4(k)}. \quad (\text{B11})$$

We then arrive at the relation

$$g_{kk}^{ab} = \frac{1}{4} [\partial_k \phi^{ab}(k)]^2. \quad (\text{B12})$$

This equation allows us to obtain the QMT from the topological winding angle for a two-band Floquet-Bloch Hamiltonian with chiral symmetry in one dimension. It unveils an interesting connection between the quantum geometry and topology in 1D systems, which is different from the case reflected in the Zak phase.

APPENDIX C: EE OF FLOQUET STATES

In this Appendix, we describe an approach to obtain the bipartite von Neumann and Rényi EE for a many-particle state of noninteracting fermions with an arbitrary filling fraction over a Floquet band in 1D systems.

We start with the general relationship between the single-particle correlation matrix and the reduced density matrix of a bipartite system, which was well established for static-free lattice models [57] and generalized also to Floquet models recently [37]. Let us consider a noninteracting many-particle system S prepared in the pure state $|\Psi\rangle$ and a subsystem A belonging to S . We can obtain the reduced density matrix of A as $\hat{\rho}_A = \text{Tr}_{\bar{A}}(\hat{\rho})$. Here $\hat{\rho} = |\Psi\rangle\langle\Psi|$ is the density matrix of whole system $S = A \cup \bar{A}$. The trace $\text{Tr}_{\bar{A}}$ is taken over the degrees of freedom belonging to the subsystem \bar{A} complementing to A . If $|\Psi\rangle$ represents a Gaussian state, we could always write [57]

$$\hat{\rho}_A = \frac{1}{Z} e^{-\hat{H}_A}, \quad Z \equiv \text{Tr}(e^{-\hat{H}_A}), \quad (\text{C1})$$

where Z is a normalization factor and \hat{H}_A is usually called the entanglement Hamiltonian [57]. Any single-particle correlation function restricted to the subsystem A can now be

evaluated as

$$C_{m,n}^A = \text{Tr}(\hat{c}_m^\dagger \hat{c}_n \hat{\rho}_A) = \frac{\text{Tr}(\hat{c}_m^\dagger \hat{c}_n e^{-\hat{H}_A})}{\text{Tr}(e^{-\hat{H}_A})}, \quad (\text{C2})$$

where $\{m, n\} \in A$ and \hat{c}_m^\dagger (\hat{c}_n) creates (annihilates) a fermion into (from) the single-particle state $|m\rangle$ ($|n\rangle$) inside the subsystem A .

Let $\{|\phi_j\rangle | j \in A\}$ be the complete and orthonormal eigenbasis of \hat{H}_A with the eigenvalues $\{\xi_j\}$, such that the entanglement Hamiltonian admits the spectral decomposition

$$\hat{H}_A = \sum_{j \in A} \xi_j \hat{\phi}_j^\dagger \hat{\phi}_j. \quad (\text{C3})$$

Here the set $\{\xi_j\}$ is usually referred to as the entanglement spectrum (ES) [83] of subsystem A . Since both $\{|n\rangle | n \in A\}$ and $\{|\phi_j\rangle | j \in A\}$ form normalized bases of the subsystem A , their corresponding creation and annihilation operators can be related to each other by unitary transformations, i.e.,

$$\hat{c}_n^\dagger = \sum_{j \in A} \phi_{nj}^* \hat{\phi}_j^\dagger, \quad \hat{c}_n = \sum_{j \in A} \phi_{nj} \hat{\phi}_j, \quad (\text{C4})$$

where $\phi_{nj} = \langle n | \phi_j \rangle$. Plugging Eqs. (C3) and (C4) into (C2) and carrying out straightforward calculations, we could reexpress the $C_{m,n}^A$ as [57]

$$C_{m,n}^A = \sum_{j \in A} \frac{\langle n | \phi_j \rangle \langle \phi_j | m \rangle}{e^{\xi_j} + 1}. \quad (\text{C5})$$

Therefore, the single-particle correlation matrix C^A admits the spectral decomposition

$$(C^A)^\top = \sum_{j \in A} \zeta_j |\phi_j\rangle \langle \phi_j|, \quad \zeta_j = \frac{1}{e^{\xi_j} + 1}. \quad (\text{C6})$$

It is now clear that there is a one-to-one correspondence between the spectrum $\{\zeta_j\}$ of C^A and the ES $\{\xi_j\}$ of \hat{H}_A , i.e.,

$$\xi_j = \ln(\zeta_j^{-1} - 1). \quad (\text{C7})$$

This relation allows us to deduce the ES, EE, and the related quantities such as mutual information of a bipartite system from the spectrum of its single-particle correlation matrix [57].

Next, we try to rewrite the reduced density matrix $\hat{\rho}_A$ in terms of C^A , which allows us to obtain the EE directly from the spectrum of correlation matrix. From Eqs. (C1), (C3), (C6), and (C7), we find

$$\frac{1}{Z} = \prod_{j \in A} (1 - \zeta_j) = \det(\mathbb{I}^A - C^A), \quad (\text{C8})$$

where \mathbb{I}^A is the identity matrix of subsystem A . Using the inverse of the transformations between different bases in Eq. (C4), i.e.,

$$\hat{\phi}_j^\dagger = \sum_{n \in A} \phi_{nj} \hat{c}_n^\dagger, \quad \hat{\phi}_j = \sum_{n \in A} \phi_{nj}^* \hat{c}_n, \quad (\text{C9})$$

we could further obtain from Eqs. (C1), (C3), and (C6) that

$$e^{-\hat{H}_A} = e^{-\sum_{m,n} \ln[(C^A)^{-1} - \mathbb{I}^A]_{m,n}^\top \hat{c}_m^\dagger \hat{c}_n}. \quad (\text{C10})$$

Putting together, we find the expression of $\hat{\rho}_A$ in terms of C^A as

$$\hat{\rho}_A = \det(\mathbb{I}^A - C^A) e^{-\sum_{m,n \in A} \ln[(C^A)^{-1} - \mathbb{I}^A]_{m,n}^\top \hat{c}_m^\dagger \hat{c}_n}. \quad (\text{C11})$$

Equivalently, in terms of the eigenvalues of C^A , we would have

$$\hat{\rho}_A = \left[\prod_{j \in A} (1 - \zeta_j) \right] e^{-\sum_{j \in A} \ln(\zeta_j^{-1} - 1) \hat{\phi}_j^\dagger \hat{\phi}_j}. \quad (\text{C12})$$

For a bipartite system $S = A \cup \bar{A}$, the λ th Rényi EE and von Neumann EE between A and \bar{A} are defined as

$$S_A^{(\lambda)} \equiv \frac{1}{1 - \lambda} \ln \text{Tr} \hat{\rho}_A^\lambda, \quad (\text{C13})$$

$$S_A \equiv -\text{Tr}(\hat{\rho}_A \ln \hat{\rho}_A) = \lim_{\lambda \rightarrow 1} S_A^{(\lambda)}. \quad (\text{C14})$$

Plugging Eq. (C12) into (C13) and (C14), we could directly find

$$S_A^{(\lambda)} = \frac{1}{1 - \lambda} \sum_{j \in A} \ln[\zeta_j^\lambda + (1 - \zeta_j)^\lambda], \quad (\text{C15})$$

$$S_A = - \sum_{j \in A} [\zeta_j \ln \zeta_j + (1 - \zeta_j) \ln(1 - \zeta_j)]. \quad (\text{C16})$$

Therefore, the spectrum $\{\zeta_j\}$ of single-particle correlation matrix C^A could provide us with complete information about the bipartite EE between the subsystem A and its complement \bar{A} for a given multiparticle Gaussian state $|\Psi\rangle$ of the whole system S . Note in passing that the relations in Eqs. (C15) and (C16) are applicable to both static and Floquet systems made up of noninteracting fermions in Gaussian states [37]. For a Floquet system with a one-period evolution (Floquet) operator \hat{U} , one could start with the multiparticle state in the form of $|\Psi\rangle = \prod_{\ell \in \text{occ.}} \hat{\psi}_\ell^\dagger |\emptyset\rangle$ and the resulting density operator $\hat{\rho} = |\Psi\rangle \langle \Psi|$, where $|\emptyset\rangle$ is the vacuum state and $\hat{\psi}_\ell^\dagger$ creates a fermion in the single-particle Floquet eigenbasis $|\psi_\ell\rangle$ of \hat{U} [37].

APPENDIX D: EE AND THE OVERLAP MATRIX

In this Appendix, we discuss an approach to obtain the EE from the overlap matrix restricted to a given subsystem [66–68], which encodes the quantum geometry of the latter [65]. We start with the Fredholm determinant

$$D^A(\zeta) \equiv \det(\zeta \mathbb{I}^A - C^A) = \prod_{j \in A} (\zeta - \zeta_j). \quad (\text{D1})$$

Here the meanings of \mathbb{I}^A , C^A , and $\{\zeta_j\}$ for subsystem A are the same as those introduced in Appendix C. Note in passing that the correlation-matrix eigenvalue ζ_j has the range $[0, 1]$ for any j . In terms of the Fredholm determinant, we could express the Rényi EE $S_A^{(\lambda)}$ in terms of a contour integration encircling the segment $[0, 1]$ of the real axis, i.e.,

$$S_A^{(\lambda)} = \oint \frac{d\zeta}{2\pi i} \frac{1}{1 - \lambda} \ln[\zeta^\lambda + (1 - \zeta)^\lambda] \frac{d \ln D^A(\zeta)}{d\zeta}. \quad (\text{D2})$$

The related von Neumann EE can further be obtained by taking the limit $\lambda \rightarrow 1$.

For any two occupied single-particle states $|\psi_\ell\rangle$ and $|\psi_{\ell'}\rangle$ in a composite system $S = A \cup \bar{A}$, their overlap within the subsystem A can be defined as

$$O_{\ell,\ell'}^A = \sum_{n \in A} \langle \psi_\ell | n \rangle \langle n | \psi_{\ell'} \rangle = \sum_{n \in A} \psi_{n\ell}^* \psi_{n\ell'}. \quad (\text{D3})$$

If we have in total N such occupied states $\{|\psi_\ell\rangle | \ell = 1, \dots, N\}$, all the quantum geometry of this state manifold

$$\text{Tr}[(O^A)^q] = \sum_{n_1, \dots, n_q} \sum_{\ell_1, \dots, \ell_q} \langle \psi_{\ell_1} | n_1 \rangle \langle n_1 | \psi_{\ell_2} \rangle \langle \psi_{\ell_2} | n_2 \rangle \langle n_2 | \psi_{\ell_3} \rangle \dots \langle \psi_{\ell_{q-1}} | n_{q-1} \rangle \langle n_{q-1} | \psi_{\ell_q} \rangle \langle \psi_{\ell_q} | n_q \rangle \langle n_q | \psi_{\ell_1} \rangle. \quad (\text{D4})$$

For the N -particle state $|\Psi\rangle = \prod_{\ell=1}^N \hat{\psi}_\ell^\dagger |\emptyset\rangle$ and for any $\ell \in \ell_1, \dots, \ell_q$, we have

$$\sum_{\ell} \langle \psi_\ell | m \rangle \langle n | \psi_\ell \rangle = \langle \Psi | \hat{c}_m^\dagger \hat{c}_n | \Psi \rangle = C_{m,n}^A, \quad (\text{D5})$$

where $m, n \in A$ and $C_{m,n}^A$ is the correlation-matrix element of subsystem A [Eq. (C2)]. Inserting Eq. (D5) into (D4), we find [after reorganizing the terms in Eq. (D4)] that

$$\text{Tr}[(O^A)^q] = \text{Tr}[(C^A)^q]. \quad (\text{D6})$$

Therefore, taking any power $q \in \mathbb{N}$, the trace of the overlap matrix O^A and the correlation matrix C^A restricted to the subsystem A are identical. Such a connection would allow us to express EE in terms of the eigenvalues of O^A , within which the quantum geometric properties of the occupied states $\{|\psi_\ell\rangle | \ell = 1, \dots, N\}$ are encoded.

To proceed, we take the logarithm of the Fredholm determinant in Eq. (D1), yielding [66–68]

$$\ln[D^A(\zeta)] = \sum_j \ln(\zeta - \zeta_j) = \sum_j \left(\ln \zeta - \sum_{q=1}^{\infty} \frac{\zeta_j^q}{q \zeta^q} \right). \quad (\text{D7})$$

Let $\{\eta_\ell | \ell = 1, \dots, N\}$ be the eigenvalues of the overlap matrix O^A , we obtain from Eq. (D6) that

$$\sum_{\ell} \eta_\ell^q = \text{Tr}[(O^A)^q] = \text{Tr}[(C^A)^q] = \sum_j \zeta_j^q. \quad (\text{D8})$$

Combining Eqs. (D7) and (D8) into (D2) finally leads us to another explicit expression for the Rényi bipartite EE $S_A^{(\lambda)}$, i.e.,

$$S_A^{(\lambda)} = \frac{1}{1-\lambda} \sum_{\ell=1}^N \ln[\eta_\ell^\lambda + (1-\eta_\ell)^\lambda], \quad (\text{D9})$$

and also for the von Neumann EE

$$S_A = - \sum_{\ell=1}^N [\eta_\ell \ln \eta_\ell + (1-\eta_\ell) \ln(1-\eta_\ell)]. \quad (\text{D10})$$

Note in passing that N here counts the total number of occupied single-particle states, which is fixed regardless of the size of subsystem A . In summary, for a given group of occupied single-particle states $\{|\psi_\ell\rangle | \ell = 1, \dots, N\}$ within a noninteracting fermionic system, we can obtain the bipartite EE through Eqs. (D9) and (D10) after getting the eigenspectrum

that are associated to the subsystem A should be captured by the $N \times N$ overlap matrix O^A with elements $\{O_{\ell,\ell'}^A | \ell, \ell' = 1, \dots, N\}$, which are given by Eq. (D3).

We could now establish a connection between the spectra of the overlap matrix O^A and the single-particle correlation matrix C^A [Eq. (C2)] [66–68], which further allows us to figure out the quantum-geometric component of EE. Let us consider the q th power of O^A , whose trace is given by

$\{\eta_\ell | \ell = 1, \dots, N\}$ of the overlap matrix O^A [Eq. (D3)]. Since O^A encodes the quantum geometry of many-particle state $|\Psi\rangle = \prod_{\ell} |\psi_\ell\rangle$, we expect to identify geometric contributions to EE from Eqs. (D9) and (D10) after removing possible nongeometric components [65]. It deserves to mention that the results developed here could be equally applicable to both static and Floquet systems. For the latter case, we simply regard $\{|\psi_\ell\rangle | \ell = 1, \dots, N\}$ as a set of occupied single-particle Floquet eigenstates of a periodically driven quantum system.

APPENDIX E: GEE OF FLOQUET STATES

In this Appendix, we discuss a scheme of decomposing EE into a geometric part (GEE) and a nongeometric contribution following Ref. [65]. We restrict our attention to the quantum geometry of 1D systems in wave-vector space. The formalism discussed here is not hard to be generalized to higher spatial dimensions and to other kinds of parameter spaces.

Let $\{|\varphi_k\rangle\}$ be a set of eigenstates populating a single Floquet-Bloch band (under PBC), the overlap matrix element in Eq. (D3) can be expressed in this case as

$$O_{k,k'}^A = \sum_{n \in A} \langle \varphi_k | n \rangle \langle n | \varphi_{k'} \rangle. \quad (\text{E1})$$

Assuming that there are L unit cells in the 1D lattice and each unit cell has p internal degrees of freedom (spins, sublattices, etc.), the wave-function overlap takes the form

$$\langle n | \varphi_k \rangle = \frac{1}{\sqrt{L}} e^{ikn} \begin{pmatrix} b_1(k) \\ \vdots \\ b_p(k) \end{pmatrix} \equiv \frac{1}{\sqrt{L}} e^{ikn} |\psi_k\rangle. \quad (\text{E2})$$

It allows us to reexpress the $O_{k,k'}^A$ in Eq. (E1) as

$$O_{k,k'}^A = \frac{1}{L} \sum_{n \in A} e^{-i(k-k')n} \langle \psi_k | \psi_{k'} \rangle. \quad (\text{E3})$$

For a subsystem A with L_A unit cells, the summation in Eq. (E3) can be worked out, yielding

$$O_{k,k'}^A = O_{k,k'}^{A_0} \langle \psi_k | \psi_{k'} \rangle, \quad (\text{E4})$$

where

$$O_{k,k'}^{A_0} = \begin{cases} L_A/L, & k = k' \\ \frac{\sin[(k-k')L_A/2]}{L \sin[(k-k')/2]} e^{i(k-k')}, & k \neq k'. \end{cases} \quad (\text{E5})$$

The coefficient $O_{k,k'}^{A_0}$ is generic and it describes the overlap matrix element of a single-band lattice model in one dimension, whose related quantum geometry is trivial in k space. Therefore, if we remove the contributions from the spectrum of O^{A_0} to EE, we will be left with the part of EE that is originated from the quantum geometry of a multiband system. Based on this understanding, we may define the Rényi GEE between two subsystems A and \bar{A} as

$$S_{\text{QG}}^{(\lambda)} = S_A^{(\lambda)} - S_{A_0}^{(\lambda)}, \quad (\text{E6})$$

where $S_A^{(\lambda)}$ and $S_{A_0}^{(\lambda)}$ are obtained by inserting the spectrum of O^A [Eq. (E4)] and O^{A_0} [Eq. (E5)] into Eq. (D9), respectively. The von Neumann EE then reads as

$$S_{\text{QG}} = S_A - S_{A_0}. \quad (\text{E7})$$

Physically, the GEE defined here characterizes the EE due to multiband quantum geometric effects [65]. It omits the contribution from a set of fermions with the same population as the multiband system but with trivial quantum geometries. We will use Eq. (E7) to describe the GEE of different Floquet models considered in the main text.

-
- [1] J. Cayssol, B. Dóra, F. Simon, and R. Moessner, Floquet topological insulators, *Physica Status Solidi RRL* **7**, 101 (2013).
- [2] M. Bukov, L. D'Alessio, and A. Polkovnikov, Universal high-frequency behavior of periodically driven systems: from dynamical stabilization to Floquet engineering, *Adv. Phys.* **64**, 139 (2015).
- [3] A. Eckardt, *Colloquium: Atomic quantum gases in periodically driven optical lattices*, *Rev. Mod. Phys.* **89**, 011004 (2017).
- [4] T. Oka and S. Kitamura, Floquet engineering of quantum materials, *Annu. Rev. Condens. Matter Phys.* **10**, 387 (2019).
- [5] M. S. Rudner and N. H. Lindner, Band structure engineering and non-equilibrium dynamics in Floquet topological insulators, *Nat. Rev. Phys.* **2**, 229 (2020).
- [6] F. Harper, R. Roy, M. S. Rudner, and S. L. Sondhi, Topology and broken symmetry in floquet systems, *Annu. Rev. Condens. Matter Phys.* **11**, 345 (2020).
- [7] S. Bandyopadhyay, S. Bhattacharjee and D. Sen, Driven quantum many-body systems and out-of-equilibrium topology, *J. Phys.: Condens. Matter* **33**, 393001 (2021).
- [8] A. de la Torre, D. M. Kennes, M. Claassen, S. Gerber, J. W. McIver, and M. A. Sentef, *Colloquium: Nonthermal pathways to ultrafast control in quantum materials*, *Rev. Mod. Phys.* **93**, 041002 (2021).
- [9] L. Zhou and D.-J. Zhang, Non-Hermitian floquet topological matter—A review, *Entropy* **25**, 1401 (2023).
- [10] D. Y. H. Ho and J. Gong, Quantized adiabatic transport in momentum space, *Phys. Rev. Lett.* **109**, 010601 (2012).
- [11] L. Jiang, T. Kitagawa, J. Alicea, A. R. Akhmerov, D. Pekker, G. Refael, J. I. Cirac, E. Demler, M. D. Lukin, and P. Zoller, Majorana fermions in equilibrium and in driven cold-atom quantum wires, *Phys. Rev. Lett.* **106**, 220402 (2011).
- [12] M. S. Rudner, N. H. Lindner, E. Berg, and M. Levin, Anomalous edge states and the bulk-edge correspondence for periodically driven two-dimensional systems, *Phys. Rev. X* **3**, 031005 (2013).
- [13] L. Zhou, C. Chen, and J. Gong, Floquet semimetal with Floquet-band holonomy, *Phys. Rev. B* **94**, 075443 (2016).
- [14] Y. Chen and C. Tian, Planck's quantum-driven integer quantum hall effect in chaos, *Phys. Rev. Lett.* **113**, 216802 (2014).
- [15] T. Kitagawa, M. A. Broome, A. Fedrizzi, M. S. Rudner, E. Berg, I. Kassal, A. Aspuru-Guzik, E. Demler, and A. G. White, Observation of topologically protected bound states in photonic quantum walks, *Nat. Commun.* **3**, 882 (2012).
- [16] M. C. Rechtsman, J. M. Zeuner, Y. Plotnik, Y. Lumer, D. Podolsky, F. Dreisow, S. Nolte, M. Segev, and A. Szameit, Photonic Floquet topological insulators, *Nature (London)* **496**, 196 (2013).
- [17] Y. Wang, H. Steinberg, P. Jarillo-Herrero, and N. Gedik, Observation of Floquet-Bloch states on the surface of a topological insulator, *Science* **342**, 453 (2013).
- [18] G. Jotzu, M. Messer, R. Desbuquois, M. Lebrat, T. Uehlinger, D. Greif, and T. Esslinger, Experimental realization of the topological Haldane model with ultracold fermions, *Nature (London)* **515**, 237 (2014).
- [19] W. Hu, J. C. Pillay, K. Wu, M. Pasek, P. P. Shum, and Y. D. Chong, Measurement of a topological edge invariant in a microwave network, *Phys. Rev. X* **5**, 011012 (2015).
- [20] L. J. Maczewsky, J. M. Zeuner, S. Nolte, and A. Szameit, Observation of photonic anomalous Floquet topological insulators, *Nat. Commun.* **8**, 13756 (2017).
- [21] K. Wintersperger, C. Braun, F. N. Ünal, A. Eckardt, M. D. Liberto, N. Goldman, I. Bloch, and M. Aidelsburger, Realization of an anomalous Floquet topological system with ultracold atoms, *Nat. Phys.* **16**, 1058 (2020).
- [22] J. W. McIver, B. Schulte, F.-U. Stein, T. Matsuyama, G. Jotzu, G. Meier, and A. Cavalleri, Light-induced anomalous Hall effect in graphene, *Nat. Phys.* **16**, 38 (2020).
- [23] S. Afzal, T. J. Zimmerling, Y. Ren, D. Perron, and V. Van, Realization of anomalous floquet insulators in strongly coupled nanophotonic lattices, *Phys. Rev. Lett.* **124**, 253601 (2020).
- [24] B. Chen, S. Li, X. Hou, F. Ge, F. Zhou, P. Qian, F. Mei, S. Jia, N. Xu, and H. Shen, Digital quantum simulation of Floquet topological phases with a solid-state quantum simulator, *Photon. Res.* **9**, 81 (2021).
- [25] K. Yang, S. Xu, L. Zhou, Z. Zhao, T. Xie, Z. Ding, W. Ma, J. Gong, F. Shi, and J. Du, Observation of Floquet topological phases with large Chern numbers, *Phys. Rev. B* **106**, 184106 (2022).
- [26] Z. Cheng, R. W. Bomantara, H. Xue, W. Zhu, J. Gong, and B. Zhang, Observation of $\pi/2$ modes in an acoustic Floquet system, *Phys. Rev. Lett.* **129**, 254301 (2022).
- [27] W. Zhu, H. Xue, J. Gong, Y. Chong, and B. Zhang, Time-periodic corner states from Floquet higher-order topology, *Nat. Commun.* **13**, 11 (2022).
- [28] S. Zhou, C. Bao, B. Fan, H. Zhou, Q. Gao, H. Zhong, T. Lin, H. Liu, P. Yu, P. Tang, S. Meng, W. Duan, and S. Zhou, Pseudospin-selective Floquet band engineering in black phosphorus, *Nature (London)* **614**, 75 (2023).
- [29] J.-Y. Zhang, C.-R. Yi, L. Zhang, R.-H. Jiao, K.-Y. Shi, H. Yuan, W. Zhang, X.-J. Liu, S. Chen, and J.-W. Pan, Tuning anomalous

- Floquet topological bands with ultracold atoms, *Phys. Rev. Lett.* **130**, 043201 (2023).
- [30] Y. Sun, X. Hou, T. Wan, F. Wang, S. Zhu, Z. Ruan, and Z. Yang, Photonic Floquet skin-topological effect, *Phys. Rev. Lett.* **132**, 063804 (2024).
- [31] J. Bloch, A. Cavalleri, V. Galitski, M. Hafezi, and A. Rubio, Strongly correlated electron-photon systems, *Nature (London)* **606**, 41 (2022).
- [32] E. Galiffi, R. Tirole, S. Yin, H. Li, S. Vezzoli, P. A. Huidobro, M. G. Silveirinha, R. Sapienza, A. Alù, and J. B. Pendry, Photonics of time-varying media, *Adv. Photonics* **4**, 014002 (2022).
- [33] S. Yin, E. Galiffi, and A. Alù, Floquet metamaterials, *eLight* **2**, 8 (2022).
- [34] R. W. Bomantara and J. Gong, Simulation of non-Abelian braiding in majorana time crystals, *Phys. Rev. Lett.* **120**, 230405 (2018).
- [35] R. W. Bomantara and J. Gong, Quantum computation via Floquet topological edge modes, *Phys. Rev. B* **98**, 165421 (2018).
- [36] P. Weinberg, M. Bukov, L. D'Alessio, A. Polkovnikov, S. Vajna, and M. Kolodrubetz, Adiabatic perturbation theory and geometry of periodically-driven systems, *Phys. Rep.* **688**, 1 (2017).
- [37] L. Zhou, Entanglement spectrum and entropy in Floquet topological matter, *Phys. Rev. Res.* **4**, 043164 (2022).
- [38] P. Törmä, Essay: Where can quantum geometry lead us? *Phys. Rev. Lett.* **131**, 240001 (2023).
- [39] D. Xiao, M.-C. Chang, and Q. Niu, Berry phase effects on electronic properties, *Rev. Mod. Phys.* **82**, 1959 (2010).
- [40] D. Vanderbilt, *Berry Phases in Electronic Structure Theory: Electric Polarization, Orbital Magnetization and Topological Insulators* (Cambridge University Press, Cambridge, UK, 2018).
- [41] S.-L. Zhu, Geometric phases and quantum phase transitions, *Int. J. Mod. Phys. B* **22**, 561 (2008).
- [42] S.-J. Gu, Fidelity approach to quantum phase transitions, *Int. J. Mod. Phys. B* **24**, 4371 (2010).
- [43] A. Carollo, D. Valenti, and B. Spagnolo, Geometry of quantum phase transitions, *Phys. Rep.* **838**, 1 (2020).
- [44] D. J. Thouless, M. Kohmoto, M. P. Nightingale, and M. den Nijs, Quantized Hall conductance in a two-dimensional periodic potential, *Phys. Rev. Lett.* **49**, 405 (1982).
- [45] F. D. M. Haldane, Model for a quantum Hall effect without landau levels: Condensed-matter realization of the "Parity Anomaly", *Phys. Rev. Lett.* **61**, 2015 (1988).
- [46] D. J. Thouless, Quantization of particle transport, *Phys. Rev. B* **27**, 6083 (1983).
- [47] N. Wang, D. Kaplan, Z. Zhang *et al.*, Quantum-metric-induced nonlinear transport in a topological antiferromagnet, *Nature (London)* **621**, 487 (2023).
- [48] S. Peotta and P. Törmä, Superfluidity in topologically nontrivial flat bands, *Nat. Commun.* **6**, 8944 (2015).
- [49] A. Gao *et al.*, Quantum metric nonlinear Hall effect in a topological antiferromagnetic heterostructure, *Science* **381**, 181 (2023).
- [50] H. Tian, S. Che, T. Xu, P. Cheung, K. Watanabe, T. Taniguchi, M. Randeria, F. Zhang, C. N. Lau, and M. W. Bockrath, Evidence for Dirac flat band superconductivity originating from quantum geometry, *Nature (London)* **614**, 440 (2023).
- [51] J. P. Provost and G. Vallee, Riemannian structure on manifolds of quantum states, *Commun. Math. Phys.* **76**, 289 (1980).
- [52] P. Zanardi, P. Giorda, and M. Cozzini, Information-theoretic differential geometry of quantum phase transitions, *Phys. Rev. Lett.* **99**, 100603 (2007).
- [53] M. V. Berry, Quantal phase factors accompanying adiabatic changes, *Proc. R. Soc. London A* **392**, 45 (1984).
- [54] P. Calabrese and J. Cardy, Entanglement entropy and quantum field theory, *J. Stat. Mech.* (2004) P06002.
- [55] L. Amico, R. Fazio, A. Osterloh, and V. Vedral, Entanglement in many-body systems, *Rev. Mod. Phys.* **80**, 517 (2008).
- [56] J. I. Latorre and A. Riera, A short review on entanglement in quantum spin systems, *J. Phys. A: Math. Theor.* **42**, 504002 (2009).
- [57] I. Peschel and V. Eisler, Reduced density matrices and entanglement entropy in free lattice models, *J. Phys. A: Math. Theor.* **42**, 504003 (2009).
- [58] P. Calabrese and J. Cardy, Entanglement entropy and conformal field theory, *J. Phys. A: Math. Theor.* **42**, 504005 (2009).
- [59] J. Eisert, M. Cramer, and M. B. Plenio, *Colloquium: Area laws for the entanglement entropy*, *Rev. Mod. Phys.* **82**, 277 (2010).
- [60] T. Grover, Entanglement entropy and strongly correlated topological matter, *Mod. Phys. Lett. A* **28**, 1330001 (2013).
- [61] N. Laflorencie, Quantum entanglement in condensed matter systems, *Phys. Rep.* **646**, 1 (2016).
- [62] M. Hermanns, Entanglement in topological systems, *arXiv:1702.01525*.
- [63] B. Zeng, X. Chen, D.-L. Zhou, X.-G. Wen, *Quantum Information Meets Quantum Matter* (Springer, New York, 2019).
- [64] M. Dalmonte, V. Eisler, M. Falconi, and B. Vermersch, Entanglement Hamiltonians: From field theory to lattice models and experiments, *Ann. Phys. (Berlin)* **534**, 2200064 (2022).
- [65] N. Paul, Area-law entanglement from quantum geometry, *Phys. Rev. B* **109**, 085146 (2024).
- [66] B.-Q. Jin and V. E. Korepin, Quantum spin chain, toeplitz determinants and the fisher-hartwig conjecture, *J. Stat. Phys.* **116**, 79 (2004).
- [67] I. Klich, Lower entropy bounds and particle number fluctuations in a Fermi sea, *J. Phys. A: Math. Gen.* **39**, L85 (2006).
- [68] P. Calabrese, M. Mintchev, and E. Vicari, Entanglement entropy of one-dimensional gases, *Phys. Rev. Lett.* **107**, 020601 (2011).
- [69] D. Gioev and I. Klich, Entanglement entropy of fermions in any dimension and the widom conjecture, *Phys. Rev. Lett.* **96**, 100503 (2006).
- [70] K. Yang, L. Zhou, W. Ma, X. Kong, P. Wang, X. Qin, X. Rong, Y. Wang, F. Shi, J. Gong, and J. Du, Floquet dynamical quantum phase transitions, *Phys. Rev. B* **100**, 085308 (2019).
- [71] D. Y. H. Ho and J. Gong, Topological effects in chiral symmetric driven systems, *Phys. Rev. B* **90**, 195419 (2014).
- [72] L. Zhou and J. Gong, Floquet topological phases in a spin-1/2 double kicked rotor, *Phys. Rev. A* **97**, 063603 (2018).
- [73] L. Zhou and J. Pan, Non-Hermitian Floquet topological phases in the double-kicked rotor, *Phys. Rev. A* **100**, 053608 (2019).
- [74] L. Zhou, Non-Hermitian Floquet topological superconductors with multiple Majorana edge modes, *Phys. Rev. B* **101**, 014306 (2020).
- [75] H. Wu, S. Wu and L. Zhou, Floquet topological superconductors with many Majorana edge modes: Topological invariants, entanglement spectrum and bulk-edge correspondence, *New J. Phys.* **25**, 083042 (2023).
- [76] W. Ma, L. Zhou, Q. Zhang, M. Li, C. Cheng, J. Geng, X. Rong, F. Shi, J. Gong, and J. Du, Experimental observation of

- a generalized thouless pump with a single spin, *Phys. Rev. Lett.* **120**, 120501 (2018).
- [77] M. Yu, P. Yang, M. Gong, Q. Cao, Q. Lu, H. Liu, M. B. Plenio, F. Jelezko, T. Ozawa, N. Goldman, S. Zhang, and J. Cai, Experimental measurement of the quantum geometric tensor using coupled qubits in diamond, *Natl. Sci. Rev.* **7**, 254 (2020).
- [78] X. Tan, D.-W. Zhang, Z. Yang, J. Chu, Y.-Q. Zhu, D. Li, X. Yang, S. Song, Z. Han, Z. Li, Y. Dong, H.-F. Yu, H. Yan, S.-L. Zhu, and Y. Yu, Experimental measurement of the quantum metric tensor and related topological phase transition with a superconducting qubit, *Phys. Rev. Lett.* **122**, 210401 (2019).
- [79] W. Zheng, J. Xu, Z. Ma, Y. Li, Y. Dong, Y. Zhang, X. Wang, G. Sun, P. Wu, J. Zhao, S. Li, D. Lan, X. Tan, and Y. Yu, Measuring quantum geometric tensor of non-abelian system in superconducting circuits, *Chin. Phys. Lett.* **39**, 100202 (2022).
- [80] N. Fläschner, B. S. Rem, M. Tarnowski, D. Vogel, D.-S. Lühmann, K. Sengstock, and C. Weitenberg, Experimental reconstruction of the Berry curvature in a Floquet Bloch band, *Science* **352**, 1091 (2016).
- [81] L. Asteria, D. T. Tran, T. Ozawa, M. Tarnowski, B. S. Rem, N. Fläschner, K. Sengstock, N. Goldman, and C. Weitenberg, Measuring quantized circular dichroism in ultracold topological matter, *Nat. Phys.* **15**, 449 (2019).
- [82] C.-R. Yi, J. Yu, H. Yuan, R.-H. Jiao, Y.-M. Yang, X. Jiang, J.-Y. Zhang, S. Chen, and J.-W. Pan, Extracting the quantum geometric tensor of an optical Raman lattice by Bloch-state tomography, *Phys. Rev. Res.* **5**, L032016 (2023).
- [83] H. Li and F. D. M. Haldane, Entanglement spectrum as a generalization of entanglement entropy: Identification of topological order in non-abelian fractional quantum hall effect states, *Phys. Rev. Lett.* **101**, 010504 (2008).